IEEE Access
Multidisciplinary | Rapid Review | Open Access Journal

Received March 27, 2020, accepted April 21, 2020, date of publication May 11, 2020, date of current version May 26, 2020.

*Digital Object Identifier 10.1109/ACCESS.2020.2993871*

# SDR Prototype for Clipped and Fast-Convolution Filtered OFDM for 5G New Radio Uplink

**SELAHATTIN GÖKCELI[1], (Student Member, IEEE), PABLO PASCUAL CAMPO[1], (Student Member, IEEE), TONI LEVANEN[1,2], (Member, IEEE), JUHA YLI-KAAKINEN[1], MATIAS TURUNEN[1], (Member, IEEE), MARKUS ALLÉN[1], TANELI RIIHONEN[1], (Member, IEEE), ARTO PALIN[2], (Member, IEEE), MARKKU RENFORS[1], (Life Fellow, IEEE), AND MIKKO VALKAMA[1], (Senior Member, IEEE)**

[1]Department of Electrical Engineering, Tampere University, FI-33720 Tampere, Finland
[2]Nokia Mobile Networks, FI-33100 Tampere, Finland

Corresponding author: Selahattin Gökceli (selahattin.gokceli@tuni.fi)

This work was supported by Nokia and Tampere University Graduate School.

**ABSTRACT** In wireless communications, higher transmission power enables higher coverage or higher data rate. However, due to hardware limitations, achieving high power efficiency becomes challenging. The main issue is that at high power region close to power amplifier (PA) saturation point the highly non-linear response of the PA leads to significant spectral regrowth. In such a case, waveforms with inherently good spectral containment allow for more spectral degradation and can be seen as the most effective solution for the problem. In this study, a fifth-generation new radio (5G NR) user equipment (UE) transmit power is improved by utilizing fast-convolution filtered orthogonal-frequency-division-multiplexing (FC-F-OFDM) waveform, which has an excellent spectral containment performance. A novel method is proposed for improving the peak-to-average-power ratio (PAPR) of FC-F-OFDM waveform, based on applying clipping before FC processing and allocating the clipping noise that stems from the applied clipping, over not only on active band, but a wider band consisting of both the in-band and guard-band regions. An accurate transmitter chain simulator including a measured memory-polynomial model of a practical PA is used to evaluate a wide set of different subcarrier spacings and channel bandwidths. Then, to validate the numerical results, a software-defined radio (SDR) based testbed is created and the modeled PA is used in this testbed. Weighted overlap-and-add (WOLA) based OFDM, also with clipping, is used as a reference in both the numerical evaluations and in measurements. For both waveforms, the transmitted signal quality, out-of-band emissions, and maximum PA output powers are measured under 5G NR specifications and results for different subcarrier spacings and channel bandwidths are provided to prove the benefits and robustness of the presented FC-F-OFDM approach.

**INDEX TERMS** Fifth-generation new radio (5G-NR), fast convolution (FC), filtered OFDM, physical layer, prototype, software-defined radio (SDR), power amplifier (PA), weighted overlap-and-add (WOLA), peak-to-average-power ratio (PAPR).

## I. INTRODUCTION

The fifth-generation New Radio (5G NR) mobile communication systems offer dramatic improvements in data rate thanks to the utilization of significantly wider channel bandwidths and new carrier frequencies [1]–[3]. Improvements in latency are also expected with the support of multiple subcarrier spacings (SCSs) in different frequency ranges and operating bands as well as by mini-slot based transmission. The 90 % spectral utilization that is achieved with current long-term evolution (LTE) systems is further improved with 5G NR. While higher spectral utilization directly increases the throughput, it also introduces more strict requirements for the filtering or time-domain windowing used to constrain spectral emissions.

Cyclic prefix (CP) orthogonal frequency-division multiplexing (OFDM) is the main physical layer radio access technology of 5G NR downlink and uplink (UL) due to its

The associate editor coordinating the review of this manuscript and approving it for publication was Wei Jiang.

advantages such as good compatibility with multiple-input multiple-output (MIMO) operation, coexistence with legacy systems, and suitability for fragmented spectrum utilization. However, CP-OFDM has also some critical limitations. As the main issues, baseline CP-OFDM has a poor spectral containment performance and, due to its high peak-to-average power ratio (PAPR), power amplifier (PA) related nonlinearities may further limit the transmission quality. Discrete Fourier transform (DFT)-precoded OFDM (also known as DFT-spread-OFDM (DFT-s-OFDM)) is widely used for addressing the PAPR issue in OFDM-based systems, especially for UL transmission in power-limited scenarios [4]. However, it also has poor spectral containment performance and it does not support MIMO operation so well as CP-OFDM, which is suitable for frequency-domain scheduling and has a straightforward receiver structure [5].

Weighted overlap-and-add (WOLA) based OFDM (WOLA-OFDM) [6], is the best known and most trivial waveform processing method to improve CP-OFDM spectral containment performance by limiting the out-of-band (OOB) emissions in the transmitter (TX) and reducing the mixed numerology interference in the receiver (RX) [7], [8]. In order to overcome the spectral leakage induced by the rectangular pulse shape of baseline CP-OFDM, a smoother and longer pulse shape is obtained in WOLA processing by cyclically extending and windowing CP-OFDM symbols. The drawback of such windowing is the overhead in time domain which, however, can be relaxed by overlap-and-add (OLA) processing between the extended symbols.

In this study, experimental implementation of clipped and fast-convolution (FC) filtered CP-OFDM (FC-F-OFDM) is described and a universal software radio peripheral (USRP)-based software-defined radio (SDR) prototype implementation is realized. As this work focuses on UL transmissions and due to WOLA-OFDM's suitability for UL TX processing, it is selected as the reference method and an SDR implementation of a WOLA-OFDM TX is also a part of this work. Comprehensive comparisons are provided by considering mean squared error (MSE), out-of-band (OOB) emissions, and adjacent-channel-leakage-ratio (ACLR) as the performance metrics following the latest 5G NR user equipment (UE) requirements for Frequency Range 1 (FR1) [9].

As mentioned, high PAPR significantly decreases the PA efficiency and baseline CP-OFDM processing results in signals with high PAPR levels. Therefore, a simple clipping is applied on CP-OFDM signals before FC or WOLA processing. Such a simple amplitude clipping mechanism is not optimal but other well-known PAPR reduction methods increase the complexity significantly. Therefore, in order to keep the UE complexity low, only clipping is preferred as the PAPR reduction method.

As the main outcome of this study, the maximum achievable transmission power levels of FC-F-OFDM and WOLA-OFDM are investigated and compared. Increasing the transmission power increases the OOB emissions of the PA and, therefore, low PAPR and good spectral containment are key factors to maximize the PA power efficiency. Good spectral containment is also essential for various 5G NR use cases with critical performance requirements, such as mixed-numerology operation.

The main novelties of this article can be summarized as follows

- A USRP-based SDR prototype is created to realize 5G NR UL transmission and to investigate the maximum achievable transmission power level of clipped FC-F-OFDM and WOLA-OFDM. Testbed is implemented based on corresponding 5G NR requirements and related performance metrics.
- Memory-polynomial PA modeling is utilized to model the PA used in the testbed. By using the obtained PA model, a simulator is created to find the optimal parameters that result in maximum transmission power levels. Accurate simulation model allows to scan more parameter combinations more easily and then representative cases are verified by the implemented SDR prototype.
- A comprehensive performance evaluation over all subcarrier spacings supported by 5G NR with all supported maximum transmission bandwidth configurations is provided by the numerical results. In the measurements, 30 kHz SCS is used and selected channel bandwidths are evaluated. In addition, OOB emissions and ACLR metrics are also considered in the evaluation.
- The CP-OFDM processing is combined with amplitude clipping and FC filtering is used to attenuate the OOB emissions caused by clipping noise. Although WOLA-OFDM cannot reduce the OOB emissions induced by clipping, we show that with moderate clipping targets, the UE transmission power can be slightly increased.
- Novel filter passband extension (FPE) method is proposed to improve the PAPR performance and transmission power level of FC-F-OFDM waveform with CP-OFDM clipping. At large, all the presented results indicate that FC-F-OFDM can provide larger transmission power than WOLA-OFDM.

The rest of the paper is organized as follows. In Section II the current state of the art is described in more detail accompanied with additional details on the novelties of this work. Then, in Section III, details of the considered waveform processing techniques applied on top of the clipped CP-OFDM waveform and PA modeling are presented. In Section IV, the USRP-based SDR prototype testbed and the evaluated 5G NR transmitter emission requirements are explained. Then, in Section V, the USRP-based SDR prototype measurement results are analyzed and discussed together with supporting numerical evaluations. Finally, the conclusions are drawn in Section VI.

## II. STATE-OF-THE-ART AND NOVELTY

In related literature, various filtering and time-domain windowing based enhancements of CP-OFDM have been extensively studied [7], [8], [10]–[15]. Subband filtering-based

CP-OFDM enhancements offer flexible design and good spectral containment performance, which are the main reasons for the popularity of these waveforms in the recent term. Nevertheless, time-domain realization of subband-filtering schemes is not efficient [12]. Furthermore, these schemes cannot be straightforwardly configured based on essential 5G NR requirements that necessitate heterogeneous configuration of different numerologies for different subbands, bandwidth parts, or channel bandwidths. These constraints limit the potentiality of these waveforms. Much of the related earlier research work has focused on evaluating waveforms that do not fulfill the transparent processing requirement specified for 5G NR implementations working on top of CP-OFDM waveforms [16]–[18]. In [19], a more similar study was conducted including experimental investigation of the effects of a non-linear PA and other hardware-related distortions on CP-OFDM, WOLA-OFDM, and block-filtered OFDM. In our work, we provide comprehensive performance evaluation over all subcarrier spacings supported by 5G NR with selected channel bandwidths representing low-, medium-, and high-performance UE devices. In addition, the most recent 3GPP specifications related to OOB emissions and ACLR requirements are fulfilled to increase the practical value of the presented results.

By targeting the issues associated with subband filtering-based waveforms, the FC-F-OFDM waveform was proposed in [12], [20]. Fast-convolution facilitates an efficient frequency-domain filtering and its combination with CP-OFDM waveforms brings significant advantages. The effective subband processing mechanism provides an excellent spectral containment performance, and channelization of different numerologies based on subband-specific requirements can easily be achieved. These advantages are quite important as the main requirements of 5G NR that are associated with the subband-specific allocation and spectral utilization can be met by FC-F-OFDM waveforms. Furthermore, FC-F-OFDM also provides a very good TX MSE performance. As another important benefit, FC-F-OFDM TX or RX processing is directly compatible with CP-OFDM TX or RX processing, respectively [21]. Furthermore, FC filtering can be used with single-carrier or precoded OFDM-based waveforms and their variants such as [22], [23]. However, in this study, only CP-OFDM is considered and use of FC filtering with other possible waveforms will be considered in the future studies.

As mentioned, WOLA-OFDM is quite effective processing in terms of spectral containment. However, its PAPR performance is not different from that of CP-OFDM. In line with this, clipping can be used and, it has been observed that combining WOLA-OFDM with simple clipping does not cause any issue as long as the targeted PAPR levels do not lead to significant OOB emissions. On the other hand, clipping combined with FC filtering inherently provides significantly better OOB emission performance but causes an increase in PAPR, as the filter effectively shapes the frequency response of the so-called peak-cancellation signal. In order to decrease this effect, a novel clipping noise allocation mechanism, so-called FPE, is proposed. Accordingly, as FC-F-OFDM allows to use very narrow guard bands, the passband of the channel filter is increased to allow wider clipping noise response, without violating the OOB requirements. As it will be shown with measurement and simulation results, FC-F-OFDM supports very low PAPR levels because it can effectively attenuate the OOB emission caused by clipping and therefore it provides higher transmission power than WOLA-OFDM, which confirms the discussion presented in [24]. For interested reader, more advanced techniques relating to, e.g., base-station implementation and enabling support for mixed-numerology signal PAPR reduction and transmission are described in [25].

The presented evaluations also require an extensive search over a large parameter set and such an extensive search in real time is not practical. Therefore, the PA used in the testbed is characterized by using a memory-polynomial PA modeling approach. This model is then used in the developed simulator to accurately model the PA distortion as observed in the implemented testbed. Parameter search is done with the simulator based on 5G NR Release 15 requirements and maximum achievable power levels are identified for each waveform. As the final step, measurements are conducted by using the created SDR prototype testbed with the identified parameters to verify the obtained simulation results. With realistic transceiver nodes and a PA that is considered to be compatible to 5G NR UE hardware, a comprehensive test environment is provided for an extensive waveform comparison.

## III. WAVEFORM AND POWER AMPLIFIER MODELING

### A. FC-F-OFDM PROCESSING

A block diagram of the implementation of FC-F-OFDM processing is shown in Fig. 1. Although in 5G NR Release 15 [3] UEs are not mandated to support multiple bandwidth parts or mixed-numerology operation, we describe the general FC-F-OFDM scheme supporting $M$ independently parameterized bandwidth parts or subbands. First, $M$ subband signals are generated with CP-OFDM processing and then multirate processing is realized with FC processing, which enables the efficient implementation of a high-order filter in frequency domain [12]. Accordingly, CP-OFDM processing that is associated with "OFDM TX processing" phase in the block diagram can be expressed for the $m$th subband with subband index $m \in \{0, 1, \ldots, M-1\}$ as

$$\bar{\mathbf{x}}_{\mathrm{t},m} = f_{\mathrm{CLIP}}\left(\mathbf{x}_{\mathrm{t},m}\right), \tag{1a}$$

where

$$\mathbf{x}_{\mathrm{t},m} = \mathrm{vec}\left(\mathbf{T}_{\mathrm{CP},m}\mathbf{W}^{-1}_{\mathrm{OFDM},m}\mathbf{X}_{\mathrm{f},m}\right). \tag{1b}$$

Moreover, $\mathbf{T}_{\mathrm{CP},m}$, $\mathbf{W}^{-1}_{\mathrm{OFDM},m}$, and $\mathbf{X}_{\mathrm{f},m}$ represent the $(L_{\mathrm{OFDM},m} + L_{\mathrm{CP},m}) \times L_{\mathrm{OFDM},m}$ CP insertion matrix, $L_{\mathrm{OFDM},m} \times L_{\mathrm{OFDM},m}$ inverse DFT (IDFT) matrix, and $L_{\mathrm{OFDM},m} \times S_m$ frequency-domain data matrix (including

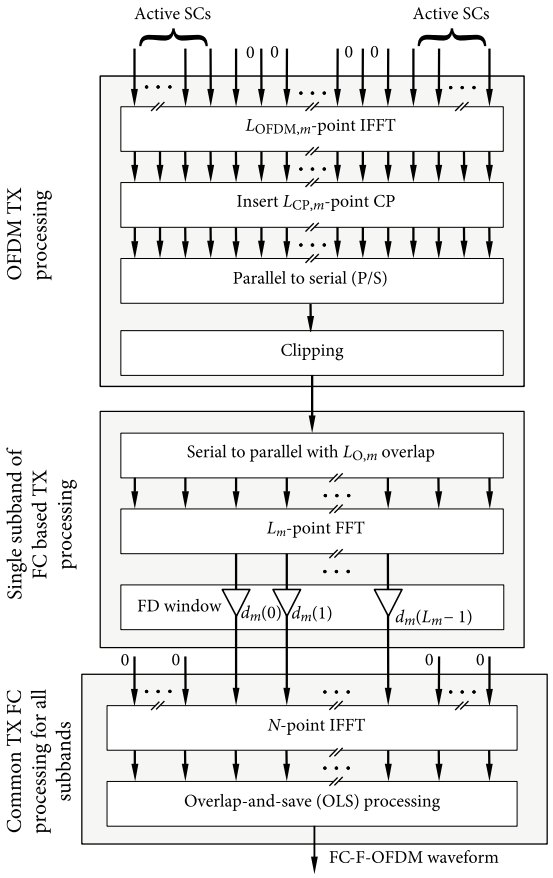


**FIGURE 1. Block diagram of the FC-F-OFDM transmitter processing for the *m*th subband.**

$L_{\mathrm{ACT},m}$ active subcarriers and zero padding) for $S_m$ OFDM symbols, respectively. Here, $L_{\mathrm{OFDM},m}$ represents the transform size of OFDM processing and in this case, it is equal to nominal transform size $L_{\mathrm{NOM},m}$, i.e., $L_{\mathrm{OFDM},m} = L_{\mathrm{NOM},m}$. Moreover, vec$(\cdot)$ represents vectorization operation, that is, vertically stacking the columns of the input matrix. Here, the columns correspond to the CP-OFDM symbols at input sample rate. In order to reduce the PAPR level of the signal, clipping is also applied in this phase and this operation is denoted as

$$f_{\mathrm{CLIP}}(x) = \begin{cases} x, & \text{if } |x| \le \gamma \\ Ae^{\angle x}, & \text{if } |x| > \gamma \end{cases} \tag{2}$$

where $\angle x$ and $|x|$ denote the phase angle and modulus of a complex number $x$, respectively. Moreover, $\gamma$ is the clipping threshold and $A$ is the amplitude threshold value that is computed as $A = \gamma\sqrt{E(|x|^2)}$ where $E(\cdot)$ represents the expectation operator. Throughout the paper, subindices t and f are used to differentiate between time-domain and frequency-domain signals, respectively.

Next, in the FC processing part that is denoted as "Single subband of FC based TX processing" in the block diagram, subband signals are divided into overlapping blocks of length $L_m$ with overlap of $L_{\mathrm{O},m}$ samples and non-overlapping blocks of length $L_{\mathrm{S},m} = L_m - L_{\mathrm{O},m}$ with the overlap factor of $\lambda = 1 - L_{\mathrm{S},m}/L_m$. It should be noted that, in this work, overlap factor of $\lambda = 1/2$ is assumed as it provides good trade-off between performance and complexity [12], [20]. Then, conversion from time to frequency domain is realized by a $L_m$-point DFT and frequency-domain subband based multirate filtering is applied. This phase can be summarized as

$$\mathbf{U}_{\mathrm{f},m} = \mathbf{M}_m\mathbf{D}_m\mathbf{P}_m^{(L_m/2)}\mathbf{W}_{\mathrm{FC},m}\mathbf{B}_{\mathrm{t},m}\Theta_m, \tag{3}$$

where $\mathbf{B}_{\mathrm{t},m}$ represents the $L_m \times R_{\mathrm{FC}}$ matrix that contains $R_{\mathrm{FC}}$ overlapping blocks taken from $\bar{\mathbf{x}}_{\mathrm{t},m}$, $\mathbf{W}_{\mathrm{FC},m}$ represents the $L_m \times L_m$ DFT matrix and $\mathbf{P}_m^{(L_m/2)}$ represents the DFT-shift matrix obtained by cyclically shifting left the $L_m \times L_m$ identity matrix by $L_m/2$ positions. Moreover, $\mathbf{D}_m$ denotes the $L_m \times L_m$ diagonal matrix that contains the frequency-domain window weights $\mathbf{d}_m$ of the $m$th subband on the main diagonal that corresponds to the DFT of a finite-length linear-phase filter impulse response. Matrix $\mathbf{M}_m$ of size $N \times L_m$ realizes mapping of input's $L_m$ frequency-domain bins to output signal's frequency-domain bins $(c_m - \lceil L_m/2 \rceil + b)_N$ for $b = 0, 1, \ldots, L_m - 1$ where $c_m$ and $(\cdot)_N$ represent the center of the $m$th subband and modulo-$N$ operation, respectively. Moreover, IDFT transform length is given as $N = N_{\mathrm{OS}}L_{\mathrm{OFDM},m}$, where $N_{\mathrm{OS}}$ represents the oversampling factor used for accurate evaluation of PAPR [26]. In addition, the diagonal matrix $\Theta_m$ of size $R_{\mathrm{FC}} \times R_{\mathrm{FC}}$ realizes the rotation of phases of the $r$th block by $[\Theta_m]_{r,r} = \exp(j2\pi r\theta_m)$ with $\theta_m = c_m L_{\mathrm{S},m}/L_m$. In this way, phase continuity between consecutive blocks is achieved. It should be noted, that the phase rotation carried out in TX FC processing is transparent to RX, that is, plain CP-OFDM processing can be used on the RX side if desired.

Finally, "Common TX FC processing for all subbands" phase in the block diagram of Fig. 1 depicts the final step of the FC processing where overlap-and-save (OLS) processing is applied and time-domain output blocks are truncated to $N_{\mathrm{S}} = (1-\lambda)N$ samples. This can be summarized as

$$\mathbf{y}_{\mathrm{t}} = \mathrm{vec}\left(\mathbf{S}_N\mathbf{W}_{\mathrm{FC}}^{-1}\sum_{m=0}^{M-1}\mathbf{U}_{\mathrm{f},m}\right), \tag{4}$$

where $\mathbf{W}_{\mathrm{FC}}^{-1}$ is the $N \times N$ IDFT matrix and $S_N$ represents the $N_s \times N$ selection matrix that selects the required $N_s$ samples corresponding to OLS processing.

In the beginning,"OFDM TX processing" module generates the corresponding number of samples that is required to match the symbol duration of $L_{\mathrm{OFDM},m}+L_{\mathrm{CP},m}$. Then, the following FC filtering modules increase the sample rate by the factor of $I_m = N/L_m = N_{\mathrm{S}}/L_{\mathrm{S},m}$. Required sample-rate conversion can be easily realized by configuring the forward and inverse transform lengths. In this way, FC processing provides a straightforward sample-rate conversion mechanism.

To show the advantages of the FC-F-OFDM waveform, its performance is compared with CP-OFDM and WOLA-OFDM in terms of power-spectral density (PSD), ACLR, PAPR, MSE, and bit-error rate (BER). The MSE

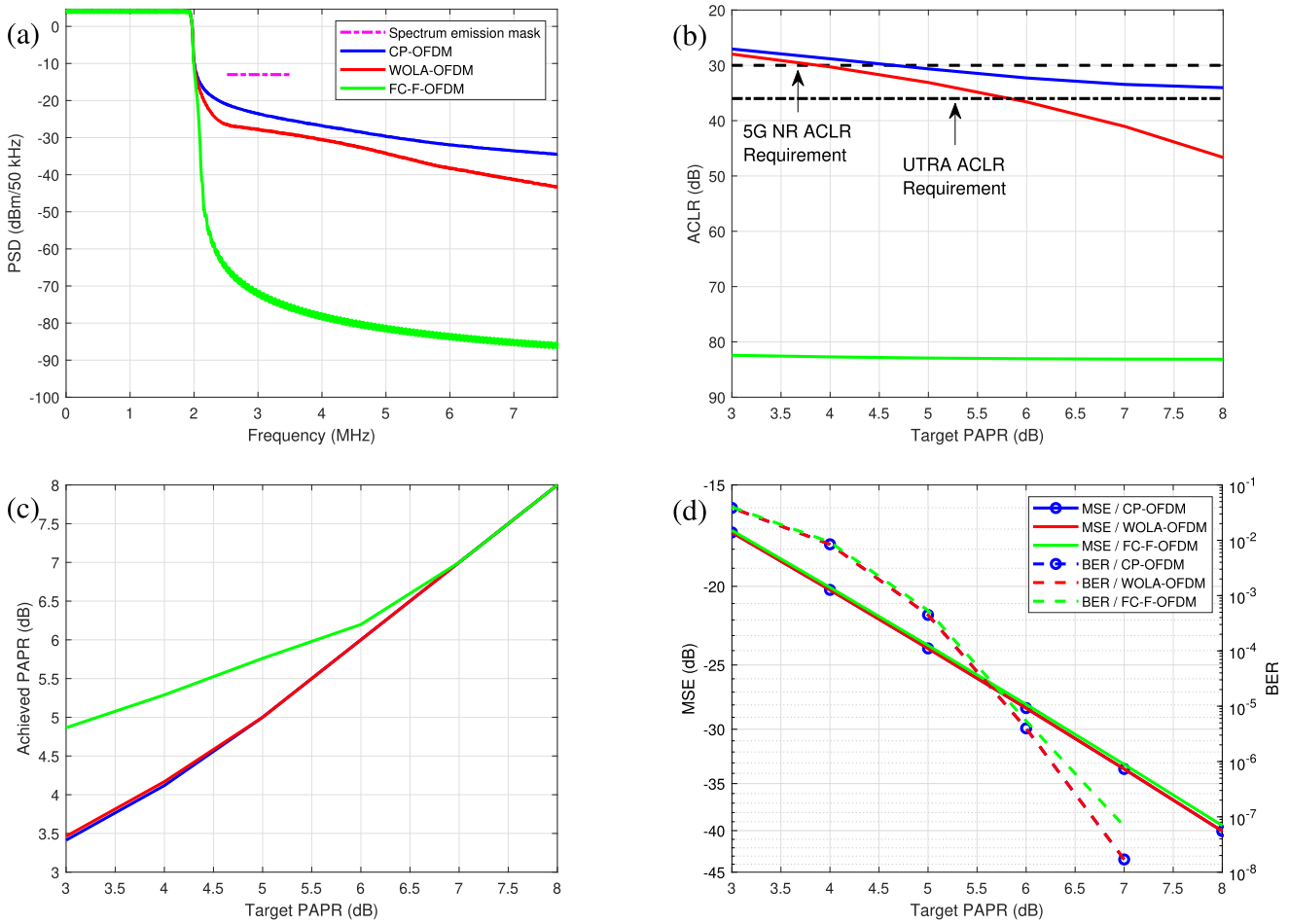


**FIGURE 2.** Simulation results of CP-OFDM, WOLA-OFDM, and FC-F-OFDM in terms of PSD, ACLR, PAPR, MSE, and BER with respect to different clipping targets, are shown for 5 MHz 5G NR channel with 30 kHz SCS in (a), (b), (c), and (d), respectively. The 5G NR and UTRA ACLR requirement thresholds are shown with dashed and dashed-dot lines in (b). The BER simulation results with 64-QAM modulation are shown using the dashed line in (d).

metric represents the average squared difference between the transmitted and the received symbols. Furthermore, ACLR metric represents the ratio of the filtered mean power of the operating 5G NR channel and the filtered mean power of an adjacent 5G NR channel [9]. In the evaluation, a 5 MHz 5G NR channel with 30 kHz SCS is considered and the other utilized parameters are given in Table 1.

Obtained simulation results are presented in Fig. 2. Firstly, PSD responses are evaluated in Fig. 2(a), by considering the clipping target of 6 dB. Here, it should be noted that passband power levels are normalized to the transmission power of 23 dBm. As can be seen, FC-F-OFDM has excellent spectral containment performance and it clearly satisfies the spectrum emission-mask requirements. On the other hand, CP-OFDM does not have a good spectral containment performance and performance of the WOLA-OFDM also degrades because of the OOB emissions caused by the clipping.

Secondly, ACLR performance with respect to different clipping targets is compared. As shown in Fig. 2(b), FC-F-OFDM has an excellent ACLR performance and even when clipping target is quite low, an ACLR value of 80 dB can be obtained. On the other hand, as expected, WOLA-OFDM has better ACLR performance than that of CP-OFDM, but it is significantly worse than that of FC-F-OFDM. Because of the limited ACLR performance, CP-OFDM is not

**TABLE 1.** The main physical layer parameters.

| Parameter | Value |
|---|---|
| Carrier frequency [GHz] | 3.5 |
| Subcarrier spacing (SCS) [kHz] | 30 |
| Physical resource block (PRB) size in subcarriers | 12 |
| Oversampling factor ($N_{\mathrm{OS}}$) | 4 |
| CP-OFDM symbols per slot | 14 |
| Number of slots averaged in the measurements | 1000 |
| FC-F-OFDM: Overlap factor | 1/2 |
| FC-F-OFDM: Number of transition band weights ($L_{\mathrm{TBW},m}$) | 4 |
| FC-F-OFDM: Transition band response | raised cosine |
| WOLA-OFDM: Window roll-off | 0.02 |
| WOLA-OFDM: Window slope response | raised cosine |
| Nonlinearity order of the MP model ($V+1$) | 7 |
| Memory of the MP model ($Q$) | 1 |
| Size of data block ($N_B$) | 219200 |

considered in the maximum transmission power evaluation. Thirdly, as shown in Fig. 2(c), CP-OFDM and WOLA-OFDM have quite good PAPR performance with clipping and, PAPR level down to 3.5 dB can be achieved. On the other hand, as explained, FC filtering causes an increase in PAPR, but still PAPR level down to 5 dB can be achieved with FC-F-OFDM. Finally, MSE and BER are evaluated together by considering different clipping targets, and 64-QAM modulation is used in this evaluation. As shown in Fig. 2(d), results are more or less same for all waveforms.

As the overall observation, plain CP-OFDM is not a feasible choice for transmission due to the limited ACLR performance, especially if we note the 36 dB UTRA ACLR requirement [9] for 5G NR and UTRA co-existence. On the other hand, ACLR performance of WOLA-OFDM is good but it is significantly worse than that of FC-F-OFDM. Because of that, a higher transmission power can be expected with FC-F-OFDM, although its PAPR performance might be the limiting factor. To understand the differences, WOLA-OFDM and FC-F-OFDM are compared shortly with a realistic simulator and also with experimental measurements to evaluate the difference in terms of the UE transmission power.

### B. FILTER PASSBAND EXTENSION

Clipping operation that is applied in ''OFDM TX processing'' module shown in Fig. 1 reduces the PAPR level effectively, but causes an increase in OOB emissions that should be limited to achieve good spectral containment performance. In the conventional iterative clipping and filtering (ICF) method [27], OOB emissions induced by clipping are removed in an iterative process of OFDM symbol-wise clipping and frequency-domain nulling of clipping noise outside active subcarriers. In the proposed model, a FC filtering based solution effectively reduces the OOB emissions. In this novel scheme, the iterative OFDM symbol-wise frequency-domain filtering phase of ICF-like methods is replaced with non-iterative FC filtering, providing much better spectral containment than conventional ICF solutions and with lower computational complexity.

The main drawback of FC filtering is the increase of PAPR. In order to balance between excellent OOB emission capabilities and the negative effect on PAPR performance, the FPE is proposed. Accordingly, the passband of the FC filter is extended to allow clipping noise at the guard bands of the channel. Guard bands are essentially extra bands reserved for transmitter induced spectral spreading and, thus, well suited for allocating the clipping noise.

An example frequency-domain window used in FC processing is illustrated in Fig. 3. The transition-band details are also shown in this figure. Similar to previous example, a 5 MHz 5G-NR channel with 30 kHz SCS is configured. The number of transition band weights is selected as eight bins and FPE size is two PRBs. The number of active PRBs is 11 and, therefore, the extended passband consists of 13 PRBs (one additional PRB on both sides of the active

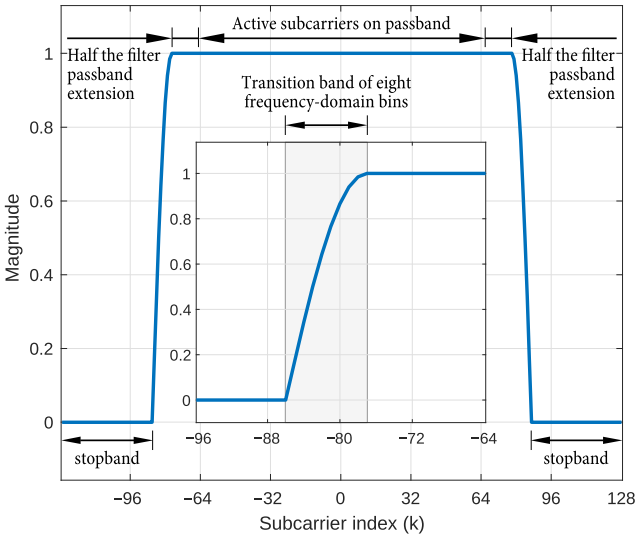


**FIGURE 3.** Illustration of frequency-domain window used in FC processing and the concept of filter passband extension.

subcarriers.) Similar to this example, with FC filtering in general and also with FPE method, the passband adjustment can easily be achieved by tuning the number of ones in the frequency-domain window corresponding to desired passband width.

In order to illustrate the concept and also analyze the performance of the proposed FPE method, an analytical model is formulated. Filtering the clipped signal is of great importance in order to satisfy the emission requirements. In line with this, the FPE method basically allows us to use a wider passband for FC filter instead of the normal passband size corresponding to band containing only the active subcarriers. In this way, improvement in PAPR performance can be expected.

To analyze the effect of FPE method on spectral containment and PAPR performance, an analytical frequency response of the filter can be used in analysis. However, in order to simplify the the derivation, an ideal frequency-domain brick-wall filter is evaluated in the theoretical analysis. First of all, analytical PSD of the clipped signal and magnitude response of the clipping noise are required. Based on the Bussgang theorem [28], $n$th sample of the clipped time-domain OFDM signal can be obtained as

$$\bar{x}_{\mathrm{t}}[n] = \alpha x_{\mathrm{t}}[n] + d_{\mathrm{t}}[n], \tag{5}$$

where $d_{\mathrm{t}}[n]$ represents the $n$th sample of the uncorrelated clipping noise and $\alpha$ represents the attenuation factor. Here, the subband index $m$ is omitted for simplicity. In line with the analytical models shown in [26] and [29], with the condition of $u \neq 0$, the autocorrelation of the clipped signal can be expressed as

$$\begin{aligned} R_{\bar{\mathbf{x}}}[u] &\triangleq E[\bar{x}_{\mathrm{t}}[n+u]\bar{x}_{\mathrm{t}}^{*}[n]] \\ &= \rho_{\mathbf{x}}[u]\big(1-\rho_{\mathbf{x}}^{2}[u]\big)^{2}\sum_{k=0}^{\infty}\rho_{\mathbf{x}}^{2k}[u]\big(k+1\big) \end{aligned}$$

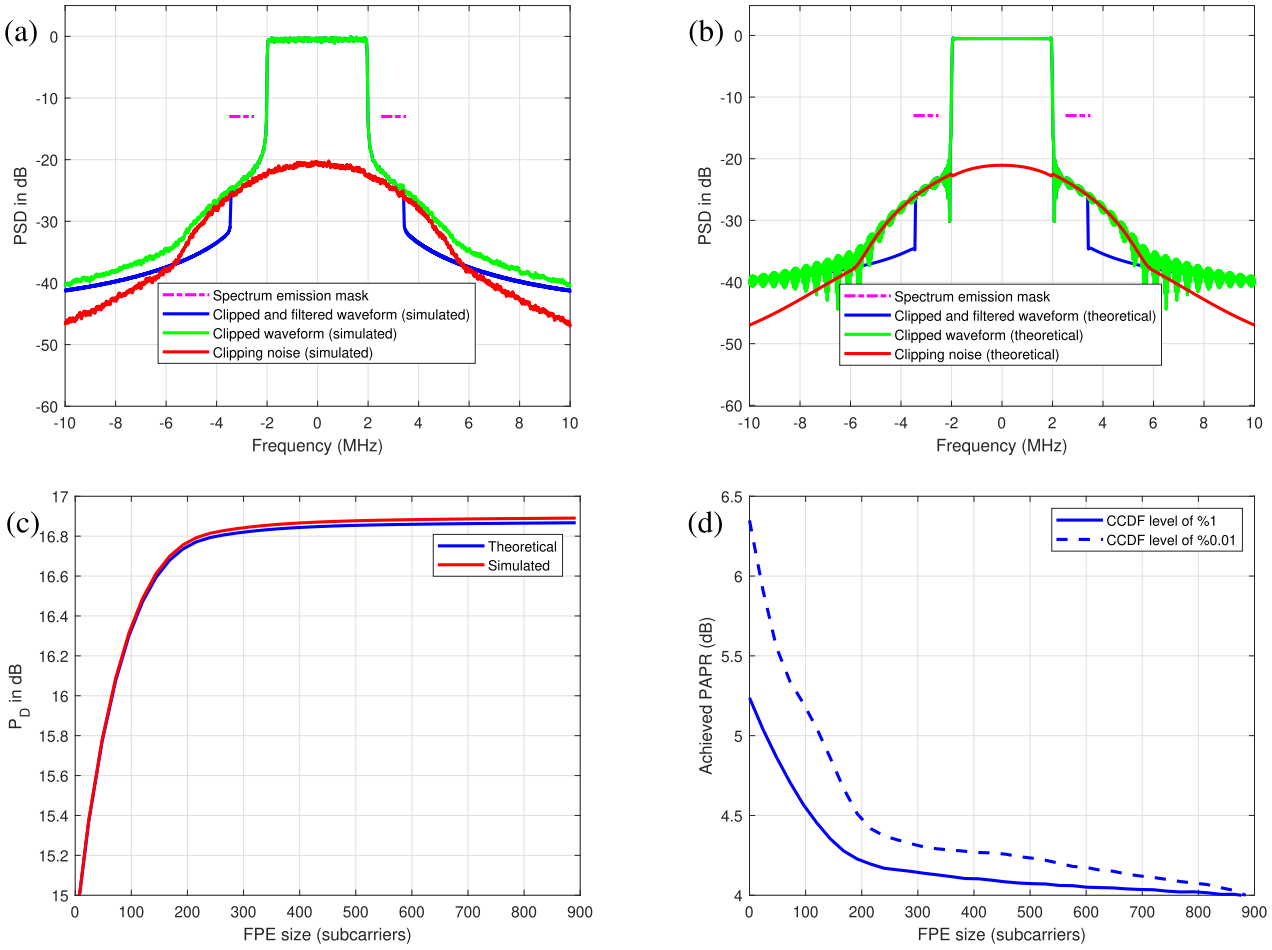


**FIGURE 4.** To illustrate the effect of FPE on the spectral containment performance of CP-OFDM, for clipping target of 3.5 dB, the simulated and analytical PSD responses are shown in (a) and (b), respectively. Moreover, simulated and analytical results are shown in (c) for total clipping noise power with respect to different FPE sizes. The PAPR performance results of FPE method for two different CCDF values are shown in (d). Here, 5 MHz NR channel and 30 kHz SCS are configured and FPE size of 8 PRBs is used in (a) and (b). In (c) and (d), different FPE sizes possible with the oversampled DFT size are evaluated.

$$\times\left\{W[u]\exp\left(\ln\Gamma(k+\frac{3}{2})-\ln\Gamma(k+2)\right)\right.$$
$$\left.\times\left(1-P\left(k+\frac{3}{2},W^2[u]\right)\right)+P\left(k+2,W^2[u]\right)\right\}^2, \tag{6}$$

where $\rho_{\mathbf{x}}[u] = R_{\mathbf{x}}[u]/R_{\mathbf{x}}[0]$ is the correlation coefficient for $u$th sample and $R_{\mathbf{x}}[u]$ represents the $u$th sample of the autocorrelation of the input OFDM signal. Moreover, $R_{\mathbf{x}}[0]$ can be expressed as $R_{\mathbf{x}}[0] = P_{\text{out}} = (1-e^{-\gamma})P_{\text{in}}$ where $P_{\text{in}}$ represents the average input power of the OFDM signal before the clipping. Besides, $\ln\Gamma(\cdot)$ and $P(\cdot)$ represent the log-gamma and incomplete gamma functions, respectively. In addition,

$$W[u] = \sqrt{\frac{\gamma}{1-\rho_{\mathbf{x}}^2[u]}}. \tag{7}$$

In line with these, correlation function of the uncorrelated clipping noise signal can be expressed as

$$R_{\mathbf{d}}[u] = R_{\tilde{\mathbf{x}}}[u] - \alpha^2 R_{\mathbf{x}}[u]. \tag{8}$$

The, PSD of the uncorrelated clipping noise can be obtained as

$$p_{\mathbf{d}}[k] = \frac{1}{N}\sum_{u=0}^{N-1} R_{\mathbf{d}}[u]\exp\left(\frac{-j2\pi ku}{N}\right). \tag{9}$$

Then total clipping noise power that is obtained after filtering with FPE can be derived as

$$P_D = \sum_{k=-L_{\text{act,ext}}/2}^{L_{\text{act,ext}}/2-1} p_{\mathbf{d}}[k], \tag{10}$$

where $L_{\text{act,ext}}$ represents the number of bins included in the extended passband.

Based on this model, analytical and simulated PSD responses are generated. Illustrations are given in Fig. 4, where PSD and PAPR performance of CP-OFDM with different FPE cases are shown. Here, a 5 MHz 5G NR channel with 30 kHz SCS is configured and target PAPR level is configured as 3.5 dB. Corresponding UL spectrum emission mask [9, Section 6] is also included for reference.

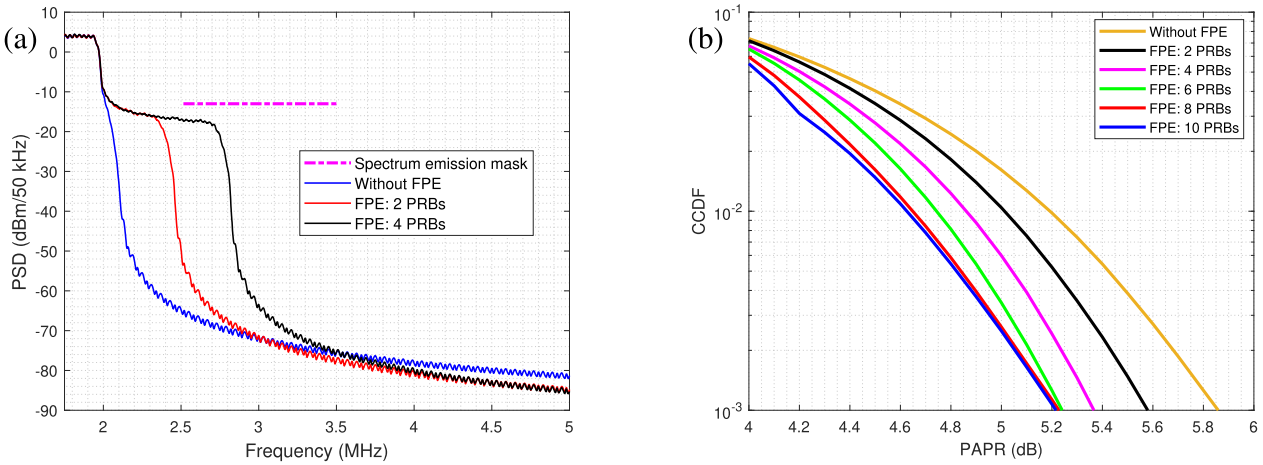


**FIGURE 5.** **(a) Simulated PSD response and (b) PAPR performance for the FC filtering based FPE method. Here, 5 MHz NR channel and 30 kHz SCS are configured whereas other utilized parameters corresponding to FC processing are given in Table 1.**

In Fig. 4(a), PSD of the clipping noise, clipped data as well as clipped and filtered data are shown. Here, rectangular filter with FPE size of 8 PRBs is used in the filtering phase and its effect on the OOB emissions can be seen from the difference between the only clipped signal and, clipped and filtered signal. Here, FPE size is equal to total number of extra PRBs in both sides, so if FPE size is equal to 8, this means that there are 4 PRBs extra in both sides. It can be seen that simulated PSD response for clipping noise given in Fig. 4(a) matches the analytical one shown in Fig. 4(b). When clipped signal is considered, it can be seen that simulated and analytical PSD responses perfectly match as well.

Similarly, as shown in Fig. 4(c), when the total power of the filtered clipping noise is considered, a good match between the simulation and analytical results can be obtained. In Fig. 4(c), total power of the clipping noise is evaluated for different sizes of FPE and match between the results holds for all considered FPE values.

In general, the selection of appropriate FPE size is vital to reduce the PAPR, as it can be seen from Fig. 4(d). Of course, maximum FPE size is limited by the channel bandwidth and allocation size, where the maximum FPE size is equal to 8 PRBs for this numerology. According to results in Fig. 4(d) which correspond to complementary, cumulative distribution function (CCDF) probability levels of 1 % and 0.01 % respectively, a significant improvement in PAPR can be obtained up to FPE size of 200 subcarriers. As a viable option, FPE size of 8 PRBs (corresponding to 96 subcarriers) also reduces the PAPR significantly and this proves the benefit of FPE method. If these results are compared with the ones shown in Fig. 4(c), it is clear that when total clipping noise power increases, the filtered PAPR decreases as well. Furthermore, these results also interpret the relation between the bandwidth of the signal with respect to the bandwidth of the clipping noise when PAPR reduction saturates. For the considered numerology, FPE size up to 200 subcarriers provides significant PAPR reduction, indicating that clipping noise most significant for PAPR reduction spans approximately 1.7 times the bandwidth of the original signal.

The FPE concept is also presented for FC processing in Fig. 5. It should be noted that "OFDM TX processing" stage remains the same, only the FC filtering step of "Single subband of FC-based TX processing" stage is modified by allocating a wider passband in the generation of frequency-domain window $\mathbf{d}_m$, as illustrated in Fig. 3. In Fig. 5, CP-OFDM parameters and PAPR target correspond to configuration in Fig. 4. When compared to the original PSD response, it can be seen that FPE sizes of two PRBs and four PRBs result in a considerable emissions in guardband and FPE size of four results in emissions outside the channel bandwidth as well. However, these FPE values do not violate the spectrum emission requirements as shown in Fig. 5(a).

Beside emission performance, PAPR performance of the method is also important. As shown in Fig. 5(b), FPE allows to reduce the PAPR of the transmitted signal. Even though the obtained improvement is limited, such an improvement might still be beneficial considering the complicated PAPR behavior of FC processing. In the following evaluations, spectral emission mask requirements and good PAPR performance are considered as main criteria and FPE sizes are configured based on these requirements. Therefore, filling the whole channel with clipping noise is targeted and the corresponding FPE size changes per SCS and channel bandwidth. Furthermore, additional PAPR reduction gain could be achieved with reduced allocation size, and the optimization of throughput performance with respect to allocation size and transmission power is an interesting topic for future studies.

In order to show the advantage of using FC filter over rectangular filter and benefit of combining it with FPE, for different FPE sizes, simulated ACLR performance of FC is compared with the analytical and simulated ACLR performance results of the CP-OFDM waveform with rectangular filter. Obtained results are presented in Fig. 6. It is clear that FC filter provides a significantly better performance than the

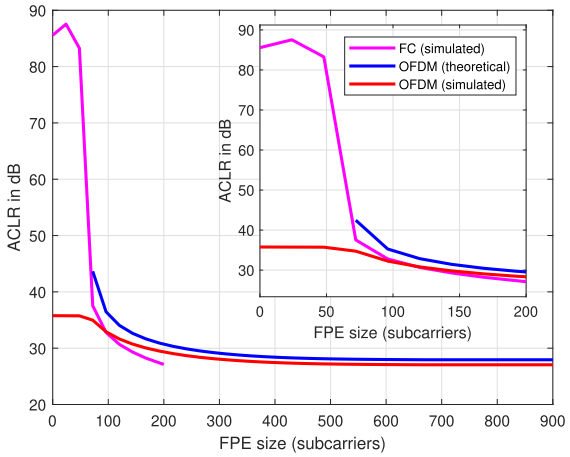


**FIGURE 6.** For the clipping target of 3.5 dB, simulated ACLR performance of FC filter and, analytical and simulated ACLR performance of CP-OFDM with rectangular filter are shown.

rectangular filter, and allows to use FPE size up to 50 subcarriers while maintaining extremely good ACLR performance. The simulator and measurement based performance evaluation are preferred to analyze the possible transmission power gains that can be obtained with FC filter and as it will be shown with different results, FC filter can support quite high transmission power levels.

### C. WOLA-OFDM PROCESSING

In the WOLA-OFDM case, oversampling is applied in CP-OFDM processing and the transform size is equal to the oversampled nominal transform size, i.e., $L_{\mathrm{OFDM},m} = N_{\mathrm{OS}} L_{\mathrm{NOM},m}$. Transmitter-side WOLA-OFDM processing can be formally defined as

$$\mathbf{y}_{\mathrm{t}} = \sum_{m=0}^{M-1} \mathbf{K}_m f_{\mathrm{CLIP}} \left( \mathrm{vec} \left( \mathbf{W}_{\mathrm{OFDM},m}^{-1} \mathbf{X}_{\mathrm{f},m} \right) \right), \qquad (11)$$

where $\mathbf{K}_m$ of size $\left(S_m(L_{\mathrm{OFDM},m} + L_{\mathrm{CP},m}) + L_{\mathrm{EXT},m}\right) \times L_{\mathrm{OFDM},m}$ is a block-diagonal matrix with $S_m$ copies of submatrix $\mathbf{O}_m$ on its main diagonal, that can be represented as

$$\mathbf{K}_m = \begin{pmatrix} \mathbf{O}_m & \cdots & \mathbf{0} \\ \vdots & \mathbf{O}_m & \vdots \\ \mathbf{0} & \cdots & \mathbf{O}_m \end{pmatrix}. \qquad (12)$$

Above submatrix $\mathbf{O}_m$ of size $L_{\mathrm{WOLA},m} \times L_{\mathrm{OFDM},m}$ implements the extension of symbol length by a length of $L_{\mathrm{CP},m} + L_{\mathrm{EXT},m}$ samples, with prefix extension of length of $L_{\mathrm{CP},m} + \frac{L_{\mathrm{EXT},m}}{2}$ and postfix extension of length of $\frac{L_{\mathrm{EXT},m}}{2}$. Accordingly, total length of extended symbol is equal to $L_{\mathrm{WOLA},m} = L_{\mathrm{OFDM},m} + L_{\mathrm{CP},m} + L_{\mathrm{EXT},m}$. The nonzero elements of $\mathbf{O}_m$ are illustrated in Fig. 8(a) and nonzero elements of $\mathbf{K}_m$ matrix are shown in Fig. 8(b) for $S_m = 3$. It should be noted that the last $L_{\mathrm{EXT},m}$ rows of preceding $\mathbf{O}_m$ matrix and first $L_{\mathrm{EXT},m}$ rows of following $\mathbf{O}_m$ matrix are placed at the same rows, representing the OLA processing. The nonzero elements of the first $L_{\mathrm{EXT},m}$ rows contain the leading edge weights of the raised-cosine window. Similarly, the nonzero elements of the last $L_{\mathrm{EXT},m}$ rows include the trailing edge weights. In summary, $\mathbf{O}_m$ can be defined as $\mathbf{O}_m = \mathbf{D}_{\mathrm{t},m}\mathbf{T}_{\mathrm{EXT},m}$, where $\mathbf{D}_{\mathrm{t},m}$ is a time-domain windowing matrix of size $L_{\mathrm{WOLA},m} \times L_{\mathrm{WOLA},m}$ that contains the time-domain weights $w_{\mathrm{t},m}[n]$ on its diagonal. Moreover, $\mathbf{T}_{\mathrm{EXT},m}$ represents the time-domain cyclic-extension matrix that is of size $L_{\mathrm{WOLA},m} \times L_{\mathrm{OFDM},m}$.

Overall, $\mathbf{K}_m$ matrix represents the TX-side WOLA processing and accordingly, the time-domain OFDM symbols are extended to symbol duration of $L_{\mathrm{WOLA},m}$, multiplied sample-wise by the time-domain window function, and concatenated using the OLA processing. These steps are shown in the block diagram given in Fig. 7. The submatrices of $\mathbf{K}_m$ contain time-domain raised-cosine window weights on the corresponding indices and realize the WOLA operation.

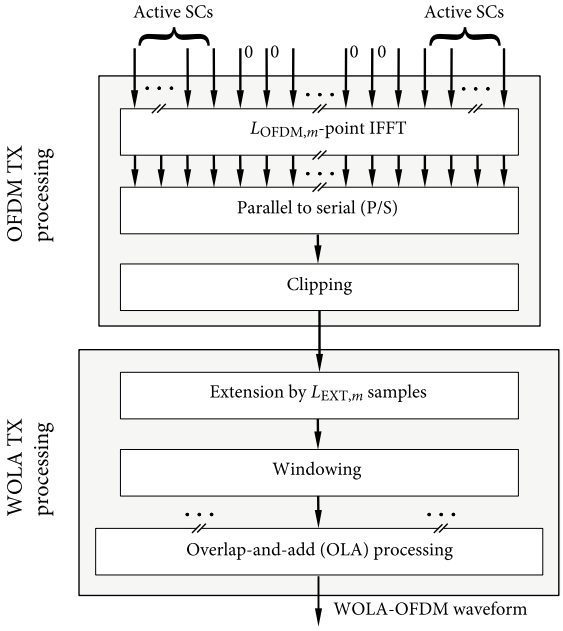


**FIGURE 7.** Block diagram for the WOLA-OFDM transmitter processing of the *m*th subband.

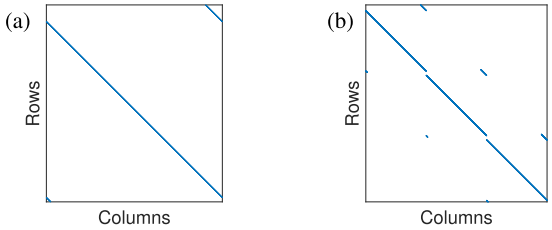


**FIGURE 8.** Nonzero elements of $\mathbf{O}_m$ and $\mathbf{K}_m$ are shown in (a) and (b), respectively.

These weights can be expressed as [7]

$$w_{\mathrm{t},m}[n] = \begin{cases} 1 - t_{\mathrm{t}}[n], & 0 \le n < \alpha L_{\mathrm{WOLA},m}, \\ t_{\mathrm{t}}[n], & (1-\alpha)L_{\mathrm{WOLA},m} \le n < L_{\mathrm{WOLA},m}, \\ 1, & \text{otherwise}, \end{cases} \tag{13}$$

where $n$ denotes the time-domain sample index, $\alpha$ represents the roll-off factor, and $t_{\mathrm{t}}[n] = \frac{1}{2}(1 + c_{\mathrm{t}}[n])$ with $c_{\mathrm{t}}[n] = \cos(\pi n/(\alpha L_{\mathrm{WOLA},m}))$.

### D. COMPUTATIONAL COMPLEXITY COMPARISON BETWEEN FC-F-OFDM AND WOLA-OFDM

In this section the computational complexity of FC-F-OFDM and WOLA-OFDM waveforms is evaluated in detail. It is assumed that both waveforms use real weighting windows and that all subbands generate the same number of samples.

The computation of an FFT or IFFT of size $L$ is assumed to take

$$\mathrm{MUL}_{\mathrm{FFT}}(L) = L[\log_2(L) - 3] + 4 \tag{14a}$$

real multiplications and

$$\mathrm{ADD}_{\mathrm{FFT}}(L) = 3L[\log_2(L) - 1] + 4 \tag{14b}$$

real additions, according to details given in [30].

FC processing requires the computation of $L_m$-point FFT and frequency-domain windowing for each of the $R_{\mathrm{FC}}$ FC blocks in the subband specific processing. Moreover, $N$-point IFFT is also needed for each of the $R_{\mathrm{FC}}$ FC blocks to create the output time-domain samples. In total, the number of real multiplications and additions required for FC-F-OFDM can be expressed as

$$\begin{aligned} &\mathrm{MUL}_{\mathrm{FC}} \\ &\quad = R_{\mathrm{FC}}\mathrm{MUL}_{\mathrm{FFT}}(N) \\ &\qquad + \sum_{m=0}^{M-1} \big(4R_{\mathrm{FC}}L_{\mathrm{TBW},m} + S_m\mathrm{MUL}_{\mathrm{FFT}}(L_{\mathrm{NOM},m}) \\ &\qquad + R_{\mathrm{FC}}\mathrm{MUL}_{\mathrm{FFT}}(L_m)\big), \end{aligned} \tag{15a}$$

$$\begin{aligned} &\mathrm{ADD}_{\mathrm{FC}} \\ &\quad = R_{\mathrm{FC}}\mathrm{ADD}_{\mathrm{FFT}}(N) \\ &\qquad + \sum_{m=0}^{M-1} \big(S_m\mathrm{ADD}_{\mathrm{FFT}}(L_{\mathrm{NOM},m}) + R_{\mathrm{FC}}\mathrm{ADD}_{\mathrm{FFT}}(L_m)\big). \end{aligned} \tag{15b}$$

In the WOLA-OFDM case, besides CP-OFDM processing, windowing process also causes some computations and the total number of real multiplications and additions required for WOLA-OFDM processing can be represented as

$$\begin{aligned} \mathrm{MUL}_{\mathrm{WOLA}} = &\sum_{m=0}^{M-1} \big(4S_mL_{\mathrm{EXT},m} \\ &+ S_m\mathrm{MUL}_{\mathrm{FFT}}(N_{\mathrm{OS}}L_{\mathrm{NOM},m})\big), \end{aligned} \tag{16a}$$

**TABLE 2. Relative complexity of FC-F-OFDM with respect to WOLA-OFDM processing (in percentage) for three SCSs and three 5G NR bandwidths.**

| Complexity | SCS | 5 MHz | 20 MHz | 100 MHz |
|---|---|---|---|---|
| Real Multiplications | 15 kHz | 267 % | 272 % | N/A |
| | 30 kHz | 264 % | 269 % | 274 % |
| | 60 kHz | N/A | 267 % | 272 % |
| Real Additions | 15 kHz | 276 % | 279 % | N/A |
| | 30 kHz | 274 % | 278 % | 280 % |
| | 60 kHz | N/A | 276 % | 279 % |

$$\begin{aligned} \mathrm{ADD}_{\mathrm{WOLA}} = &2(M-1)S_mN_{\mathrm{OS}}L_{\mathrm{NOM},m} \\ &+ \sum_{m=0}^{M-1} \big(2(S_m - 1)L_{\mathrm{EXT},m} \\ &+ S_m\mathrm{ADD}_{\mathrm{FFT}}(N_{\mathrm{OS}}L_{\mathrm{NOM},m})\big). \end{aligned} \tag{16b}$$

A complexity comparison based on these expressions is given in Table 2. In this analysis, parameters given in Table 1 are utilized with three different 5G NR transmission bandwidth configurations corresponding to 5 MHz, 20 MHz, and 100 MHz channel bandwidths [9]. Moreover, two different SCS cases that are 15 kHz and 60 kHz are also evaluated. According to results, the real multiplications and additions required by FC-F-OFDM are approximately 2.7 and 2.8 times the complexity of WOLA-OFDM, respectively. However, this study focuses on the single-subband case, which is in favor of WOLA-OFDM in terms of complexity. When multiple subbands are configured, the difference decreases as WOLA requires separate, oversampled OFDM transform for each of the $M$ subbands. Besides, when considering the performance, in most cases FC-F-OFDM provides significantly better results, as will be shown in Section V.

### E. POWER AMPLIFIER MODEL

In general, PA behavioral modeling refers to the extraction of a mathematical representation that approximates the transfer function of a PA under certain conditions [31]. Such model can be extracted based on the input and measured output data samples of the PA. Consequently, the RF circuit of the PA itself can be seen as a black box, avoiding the modeling of a complex analog circuit.

In order to extract the desired behavioral model of an arbitrary device under test (DUT), it should first be excited under appropriate operating conditions, as its behavior could vary when measuring at a different operating point. For example, the behavior of the DUT could change when excited with different input power levels, PAPR values, bandwidth, temperature, etc. In this work, different PA models have been specifically measured for different power levels and for different PAPR values, in order to provide realistic environment for the simulator.

Once the DUT is correctly excited, some specific mathematical formulation for the model needs to be chosen.

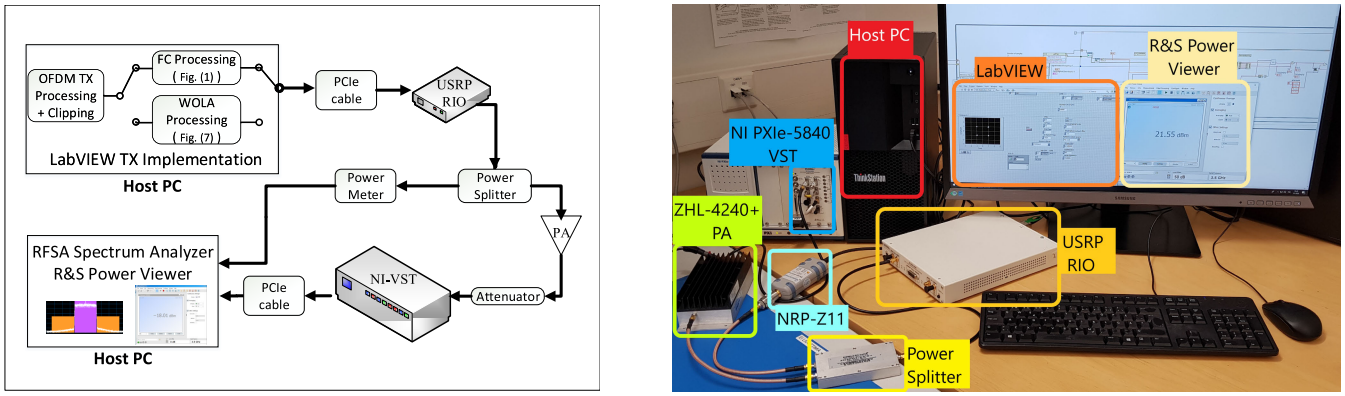


**FIGURE 9.** Block diagram and photograph of the considered USRP-based SDR prototype measurement setup are shown in (a) and (b), respectively.

There is a vast study of this topic in the literature [32], where different approaches have been compared. The key idea regarding these methods is to get an acceptable modeling performance–complexity trade-off, according to the desired application. In our work, we have adopted the memory-polynomial (MP) model to extract the PA behavior. In general, the MP model has been proven to provide good modeling performance, while maintaining a moderate level of complexity [33]. It can be expressed mathematically as

$$z_{\mathrm{t}}[n] = \sum_{q=0}^{Q} \sum_{v=0}^{W} [\boldsymbol{\beta}_{\mathrm{PA}}]_{(q(W+1)+v+1)} y_{\mathrm{t}}[n-q]\,|y_{\mathrm{t}}[n-q]|^{2v}, \quad (17)$$

where $y_{\mathrm{t}}[n]$ and $z_{\mathrm{t}}[n]$ represent the input and output signals of the DUT, $V = 2W$ with $W \in \mathbb{N}$ is the considered nonlinearty order, and $Q$ represent the memory of the MP model whereas vector $\boldsymbol{\beta}_{\mathrm{PA}}$ of size $(Q+1)(W+1) \times 1$ contains the coefficients to be extracted, modeling the behavior of the PA. Here, the notation $[\boldsymbol{\beta}_{\mathrm{PA}}]_{(p)}$ denotes the $p$th element of the vector $\boldsymbol{\beta}_{\mathrm{PA}}$. As the input and output signals are known, $\boldsymbol{\beta}_{\mathrm{PA}}$ can be straightforwardly extracted by fitting techniques. In this work, the block-based least squares (LS) approach has been used for solving the direct model parameters, considering a data block of size $N_B$, as

$$\boldsymbol{\beta}_{\mathrm{PA}} = (\boldsymbol{\Phi}_{\mathrm{t}}^{\mathsf{H}} \boldsymbol{\Phi}_{\mathrm{t}})^{-1} \boldsymbol{\Phi}_{\mathrm{t}}^{\mathsf{H}} \mathbf{z}_{\mathrm{t}}, \quad (18)$$

where $\mathbf{z}_{\mathrm{t}}$ is the output data vector, and $\boldsymbol{\Phi}_{\mathrm{t}}$ contains the PA input basis functions matrix, in this case the linear and nonlinear polynomials up until sixth order, for each time instant $n$. Formally, the basis function matrix of size $N_B \times (Q+1)(W+1)$ can be expressed as

$$\boldsymbol{\Phi}_{\mathrm{t}} = \begin{bmatrix} \boldsymbol{\phi}_{0,0} & \boldsymbol{\phi}_{1,0} & \cdots & \boldsymbol{\phi}_{W,0} & \\ \boldsymbol{\phi}_{0,1} & \boldsymbol{\phi}_{1,1} & \cdots & \boldsymbol{\phi}_{W,1} & \cdots \\ \boldsymbol{\phi}_{0,Q} & \boldsymbol{\phi}_{1,Q} & \cdots & \boldsymbol{\phi}_{W,Q} \end{bmatrix}, \quad (19a)$$

where

$$\boldsymbol{\phi}_{v,q} = \begin{pmatrix} y_{\mathrm{t}}[n-q]\,|y_{\mathrm{t}}[n-q]|^{2v} \\ y_{\mathrm{t}}[n-q+1]\,|y_{\mathrm{t}}[n-q+1]|^{2v} \\ \vdots \\ y_{\mathrm{t}}[n+N_B-1-q]\,|y_{\mathrm{t}}[n+N_B-1-q]|^{2v} \end{pmatrix}. \quad (19b)$$

## IV. TESTBED DETAILS

### A. SDR PROTOTYPE MEASUREMENT SETUP

An SDR-based testbed is created to extensively analyze the maximum achievable transmission power and also to measure different performance metrics. In this testbed, UL transmission scenario is evaluated and both FC-F-OFDM and WOLA-OFDM waveforms are implemented. The block diagram and photograph of the testbed are shown in Fig. 9. In this testbed, a host PC takes care of TX baseband signal processing using LabVIEW environment. This includes CP-OFDM signal generation with clipping to reduce the PAPR level as well as FC or WOLA processing steps. After the host PC has generated the baseband signal, these pre-calculated I/Q samples are transferred to NI USRP-2954 RIO SDR via PCIe x4 connection. The USRP supports the considered carrier frequency of 3.5 GHz and instantaneous bandwidth up to 160 MHz [34], and in this testbed it is used for implementing UE TX. This includes RF modulation and pre-amplification.

The RF signal transmitted by the USRP is fed into 3 dB power splitter in order to divide it between a Rohde & Schwarz (R&S) NRP-Z11 power meter and an external PA. This enables simultaneous signal transmission and power monitoring. The main reasons of power measurement are to validate that the signal power fluctuations are below 0.2 dB and that all the transmitted signals have the same power level. The NRP-Z11 power meter supports an input power up to 23 dBm and frequency range from 10 MHz to 8 GHz [35]. The R&S Power Viewer tool is used for monitoring the measured power level with the host PC to which the power meter is connected with an USB cable. The PA of the testbed is Mini-Circuits ZHL-4240+ that provides 42 dB gain with a high third-order output intercept point (OIP3) of 38 dBm

in the operating carrier frequency of 3.5 GHz and it supports operation in frequencies from 0.7 GHz to 4.2 GHz [36].

The testbed uses NI PXIe-5840 vector signal transceiver (VST) as an RX and it supports instantaneous bandwidth up to 1 GHz [37] making it suitable for evaluating 5G NR OOB emissions and 5G NR ACLR. The VST tolerates input power up to 33 dBm, but in order to guarantee that the receiver is working on its linear region, a 34 dB attenuator is used between the PA and the VST. The baseband signal processing of the received signal is performed on the host PC and corresponding performance metrics are evaluated. In the reception phase, estimation and correction of timing offset and carrier frequency offset are achieved by exploiting correlation between CP portions [38]. Moreover, comb-type pilot allocation with one-dimensional frequency-domain interpolation is utilized to estimate the channel, followed by zero-forcing equalization [39]. Here, we prefer using comb-type structure because we focus on CP-OFDM based UL in this study. The comb-type allocation is realized by allocating every sixth subcarrier as the pilot tone and channel coefficients for five data tones are estimated by using two successive pilot tones in the interpolation.

All the processing occurring on the host PCs are implemented using LabVIEW environment with necessary hardware and communications libraries. It is worth noting that the host PCs use offline processing for generating/processing a single data block that goes through the actual communications hardware. This is a valid approach for fast and flexible high-bandwidth waveform prototyping without the need for more laborious and expensive real-time FPGA or ASIC implementation.

### B. 5G NR UE TRANSMITTER RF EMISSION REQUIREMENTS

The 5G NR ACLR is determined as the ratio of the filtered mean power of the operating 5G NR channel and the filtered mean power of an adjacent 5G NR channel [9]. In the calculation of channel powers, measurement bandwidth is configured to be equal to maximum transmission configuration size that corresponds to each bandwidth plus one SCS based on the smallest SCS supported in that channel bandwidth [9]. For example, for a 5 MHz channel, 25 PRBs with 15 kHz SCS are supported corresponding to 4.5 MHz bandwidth and with the addition of 15 kHz, the measurement bandwidth of 4.515 MHz is obtained. The additional SCS is used due to the configurable half of a subcarrier shift in 5G NR UL. For all considered bandwidth cases, ACLR evaluation is realized based on following the details presented in [9].

In this study, a spectrum emission mask is implemented according to [9] corresponding to 5G NR OOB spectrum emission mask for UEs operating in FR1. Accordingly, the spectrum emission mask contains two different regions, namely regions within distance of 1 MHz and larger than 1 MHz from the channel edge, respectively. In the former case, measurement filter bandwidth is configured to be 1 % of the channel bandwidth and spectrum emission limit is set to −13 dBm for the channel bandwidths of 5 MHz to 40 MHz. When larger channel bandwidths are utilized, measurement filter bandwidth and the emission limit are configured as 30 kHz and −24 dBm, respectively. In the latter case, where distances larger than 1 MHz from the channel edge are considered, measurement bandwidth of 1 MHz is configured and the corresponding attenuation target depends on the distance to the channel edge and the channel bandwidth as defined in [9, Table 6.5.2.2-1].

## V. SIMULATION AND TESTBED MEASUREMENT RESULTS

In order to characterize the maximum transmission power levels that can be obtained with FC-F-OFDM and WOLA-OFDM, different cases are numerically evaluated by using the created simulator and obtained results are compared with measurement results. This comparison is essential to obtain accurate results, since the created PA model and various hardware-related uncertainties might lead to biased simulation results. With the simulator, all possible 5G NR transmission bandwidth configurations have been evaluated and results corresponding to the highest transmission power levels are presented for each bandwidth configuration in Table 3. In the measurements, three different 5G NR bandwidth configurations are considered with only the SCS value of 30 kHz. As it will be shown, results are more or less similar for all subcarrier spacings, therefore considering bandwidths of 5 MHz, 20 MHz, and 100 MHz with 30 kHz SCS as example cases is sufficient to understand the performance differences between the two evaluated waveforms. Here, the number of allocated PRBs for these bandwidth configurations are 11, 51 and 273, which correspond to the transmission bandwidth of 3.96 MHz, 18.36 MHz and 98.28 MHz. Remaining band within the channel bandwidth is allocated as guard band on both sides of the channel [9].

The parameters used in simulations and experiments are given in Table 1. As the performance metrics, the level of OOB emissions as well as ACLR and MSE metrics are evaluated and the maximum transmission power level that fulfills all 5G NR requirements corresponding to these metrics is selected. In this study, MSE of −15 dB that is the MSE requirement of QPSK modulation, and 5G NR ACLR of 30 dB that corresponds to the ACLR requirement for power class 3 devices PA [9], are considered. For the evaluation of MSE, a CP-OFDM receiver is implemented and measurement is conducted by following the 3GPP measurement guidelines defined in [9]. Moreover, PAPR levels from 2 to 8 dB are targeted as the clipping levels and results are presented for each level. Based on the obtained numerical results, a narrower PAPR interval is determined for each waveform and used in measurements. As supportive results, PAPR performance results of waveforms with respect to target PAPR levels are also presented.

The PSD responses shown in this section for measurement cases are extracted from spectrum analyzer. To remove the effect of the attenuator used in the testbed, power levels

**TABLE 3.** Maximum transmission powers (dBm) based on numerical evaluations and achieved with each waveform, shown for three different SCS cases and all possible 5G NR bandwidth configurations.

| Waveform | SCS | 5 MHz | 10 MHz | 15 MHz | 20 MHz | 25 MHz | 30 MHz | 40 MHz | 50 MHz | 60 MHz | 70 MHz | 80 MHz | 90 MHz | 100 MHz |
|---|---|---|---|---|---|---|---|---|---|---|---|---|---|---|
| FC-F-OFDM | 15 kHz | 26.5 | 26.4 | 25.9 | 26.7 | 26.1 | 25.9 | 26.3 | 26.2 | N/A | N/A | N/A | N/A | N/A |
| | 30 kHz | 26.6 | 26.6 | 25.9 | 26.5 | 26.2 | 25.9 | 26.2 | 26.3 | 25.9 | 26.4 | 26.4 | 26.4 | 26.3 |
| | 60 kHz | N/A | 26.3 | 25.8 | 26.7 | 26.2 | 25.9 | 26.2 | 26.4 | 26.1 | 26.4 | 26.4 | 26.4 | 26.3 |
| WOLA-OFDM | 15 kHz | 25.2 | 25.0 | 25.0 | 25.1 | 25.0 | 25.0 | 24.8 | 25.0 | N/A | N/A | N/A | N/A | N/A |
| | 30 kHz | 25.4 | 25.2 | 25.2 | 25.3 | 25.0 | 25.1 | 24.8 | 25.0 | 25.0 | 24.8 | 24.8 | 24.8 | 25.1 |
| | 60 kHz | N/A | 25.3 | 25.5 | 25.5 | 25.3 | 25.2 | 24.8 | 25.0 | 25.0 | 24.8 | 24.8 | 24.8 | 25.1 |

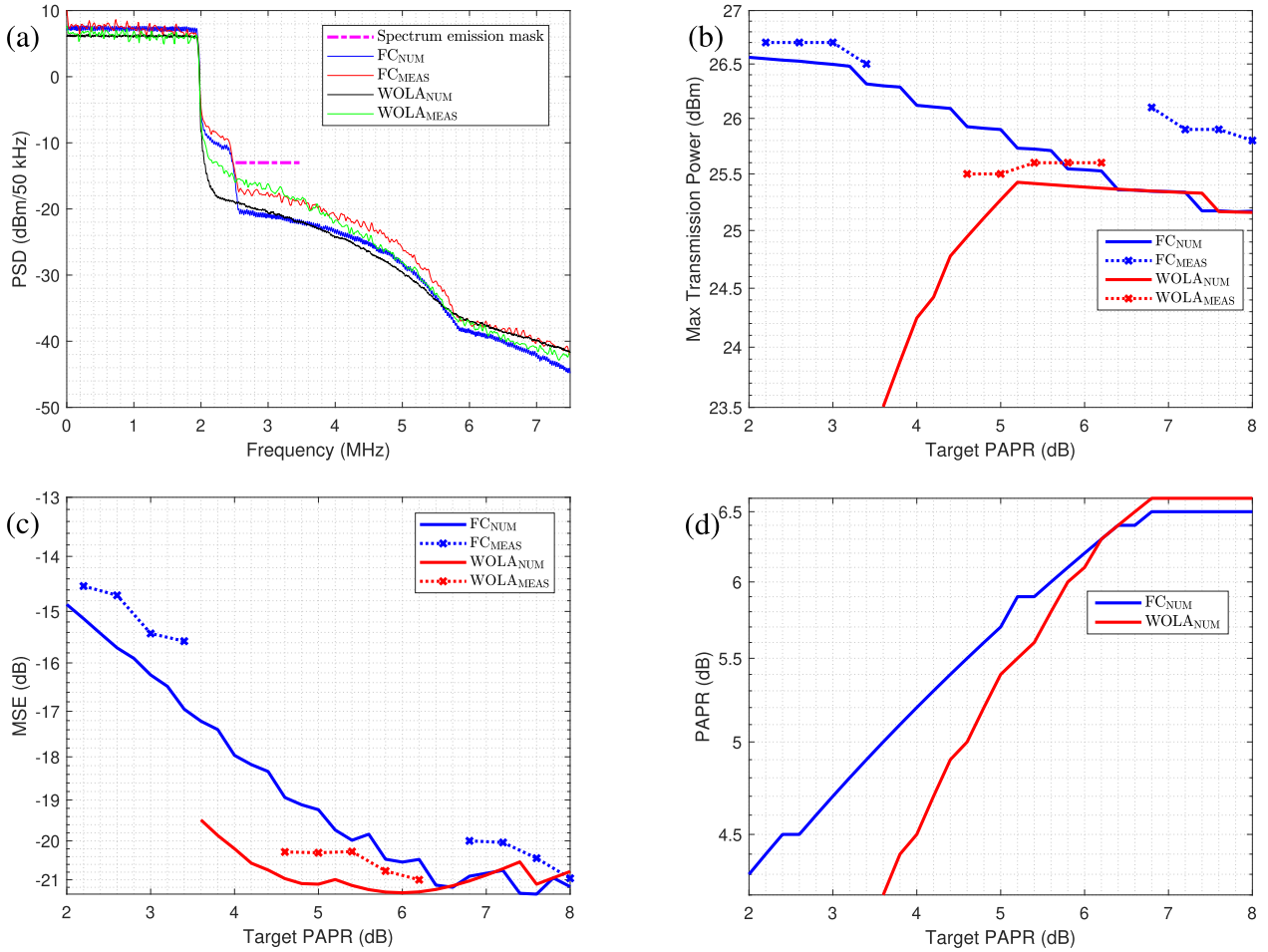


**FIGURE 10.** Obtained PSD responses with respect to spectrum emission mask, maximum transmission power levels, MSE results, and achieved PAPR levels with respect to target PAPR levels are shown for 5 MHz 5G NR channel with 30 kHz SCS in (a), (b), (c), and (d), respectively. Both simulation-based and measured results are shown in (a)-(c).

of samples are normalized based on the used attenuation level and the normalized PSD responses are shown in the corresponding figures.

First, numerical results that are obtained with the simulator, for all possible 5G NR bandwidth configurations and SCS cases are presented in Table 3. Accordingly, SCS configuration does not render any clear difference and similar results are obtained with each SCS case. The general trend is that FC-F-OFDM supports higher power levels than WOLA-OFDM in all cases. The average difference is over 1 dB, which is a significant gap, showing the effectiveness of the FC-F-OFDM waveform. In order to validate these results, experimental performance is also measured for three different bandwidth configurations of 5 MHz, 20 MHz, and 100 MHz with 30 kHz SCS, and these measurements are compared with the simulation results presented in Table 3.

As the first measurement case, performance is measured for a 5 MHz channel and corresponding results are shown

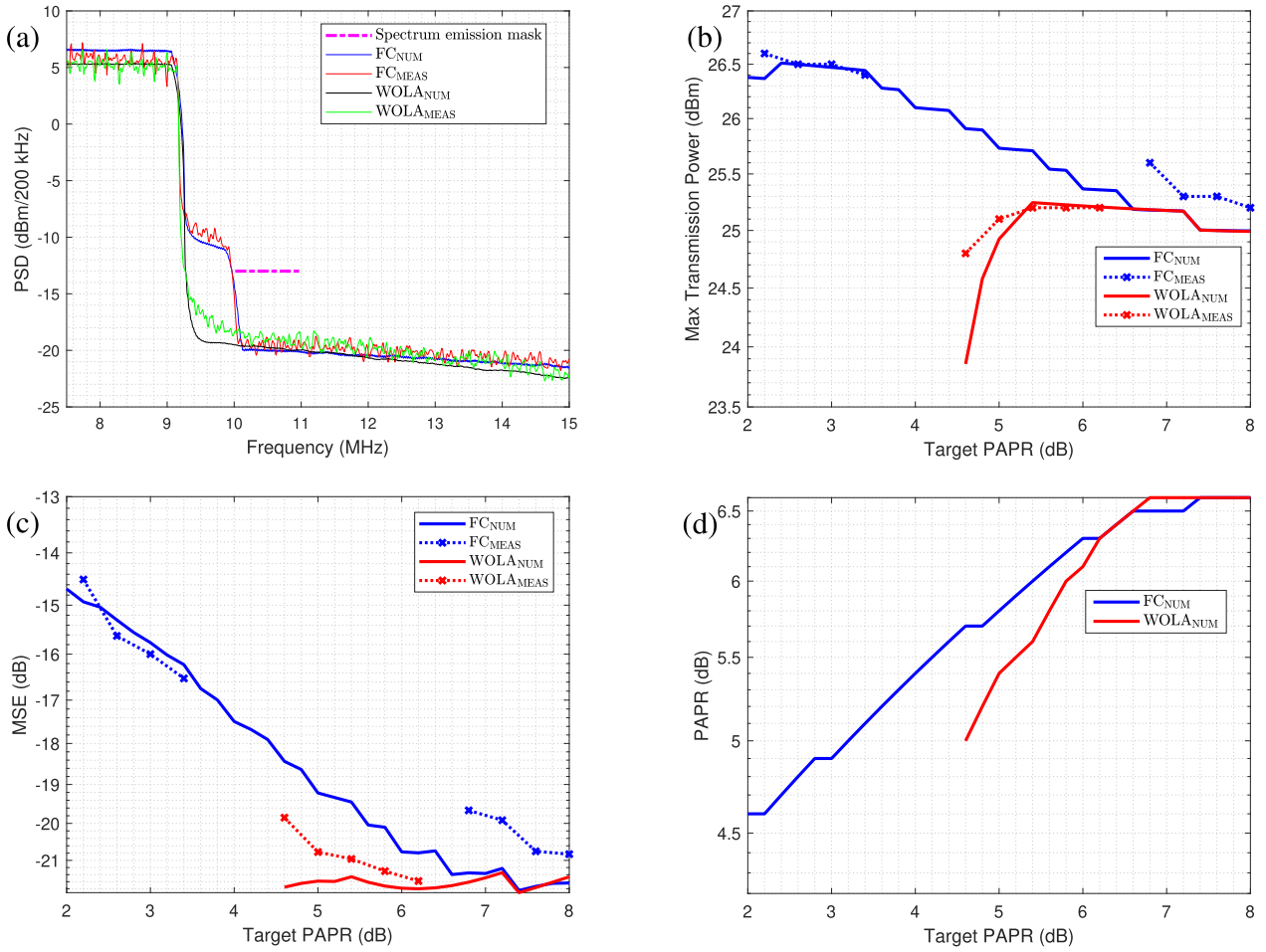


**FIGURE 11.** Obtained PSD responses with respect to spectrum emission mask, maximum transmission power levels, MSE results, and achieved PAPR levels with respect to target PAPR levels are shown for 20 MHz 5G NR channel with 30 kHz SCS in (a), (b), (c), and (d), respectively. Both simulation-based and measured results are shown in (a)-(c).

in Fig. 10. Obtained PSD responses are given in Fig. 10(a). In the generation of these responses, the maximum transmission power level setting that provides the necessary ACLR and MSE performance results is selected and PSD responses that correspond to these cases are presented. As a reference, 5G NR UL spectrum emission mask is also shown. It can be seen that the FC-F-OFDM waveform provides a higher transmission power and achieves better emission behavior, where the effectiveness of the FPE scheme is also observed. The difference between transmission power levels can be seen from Fig. 10(b). The numerical results show that the FC-F-OFDM waveform achieves higher transmission power level when clipping level is selected to be quite low i.e., 3 dB. Here, it should be noted that FC processing causes an increase in PAPR and the targeted PAPR level cannot be achieved, as can be seen from Fig. 10(d). In the WOLA-OFDM case, PAPR targets between 5 dB and 7 dB provide the highest transmission power levels. According to the obtained results of all bandwidth configuration cases, experimenting an interval of 5.5 dB to 6.5 dB in the measurements is the optimal choice for WOLA-OFDM and this interval usually provides the maximum power level among all possible PAPR target levels.

The measured and simulated results match well in the FC-F-OFDM case when low PAPR targets from 2 to 3.5 dB are considered. However, the simulator cannot accurately model FC-F-OFDM's performance when higher PAPR target levels are considered, where a difference up to 0.8 dB is observed between measurement and simulation results. In the WOLA-OFDM case, this difference is smaller but still observable. It should be noted that the PA model was created with a 20 MHz channel and mismatches in results corresponding to other channel configurations can be partially explained with this fact. As expected, targeting low PAPR levels increases MSE, which can be observed from Fig. 10(c). Utilization of a low-order modulation scheme such as QPSK is assumed when aiming for maximum power transmission, and the corresponding 5G NR MSE requirement of $-15$ dB should be targeted with QPSK modulation. WOLA-OFDM's MSE results are always below $-15$ dB and QPSK modulation can be supported with each level. On the other hand, PAPR target levels below 3 dB result in high MSE for

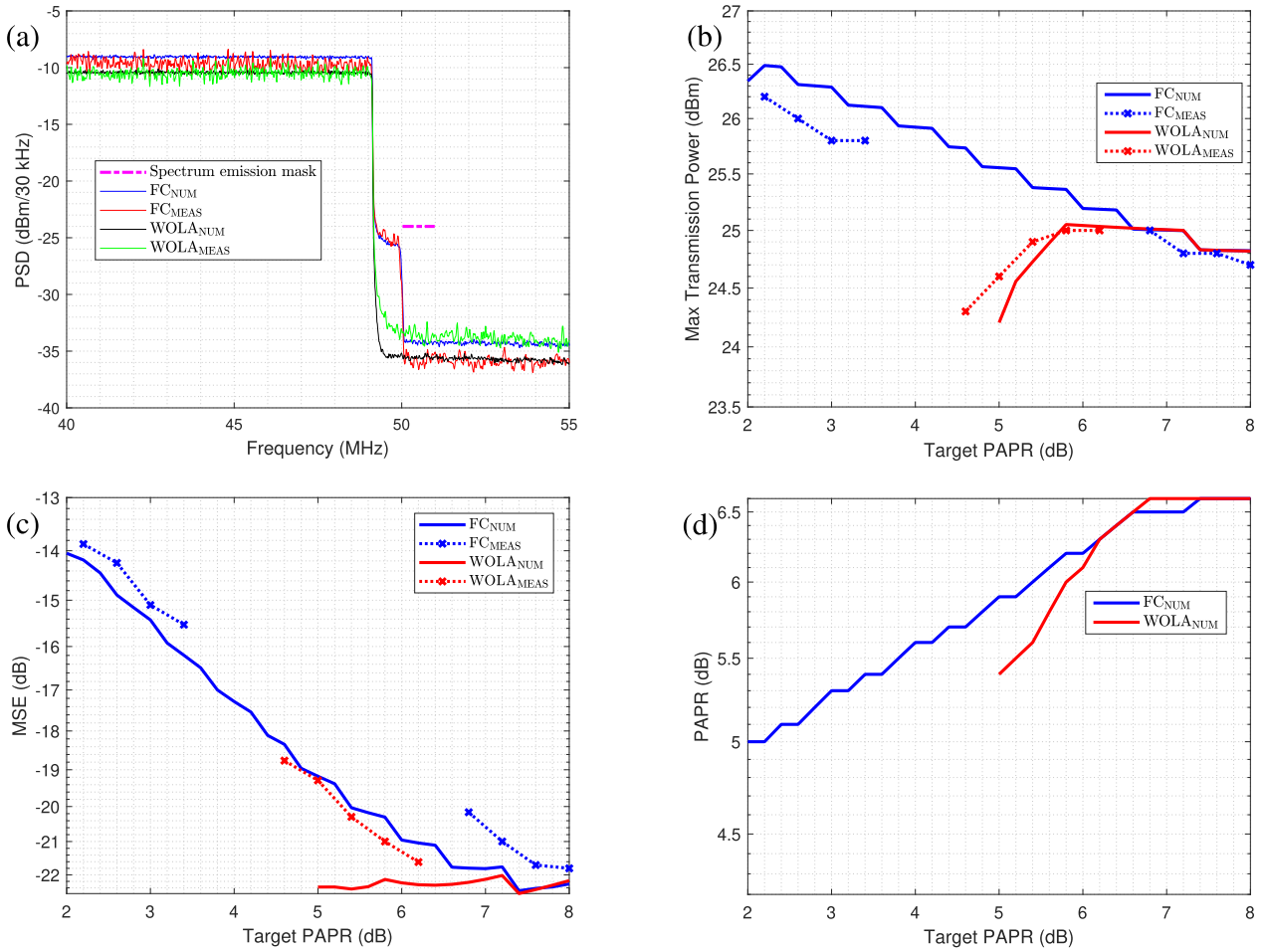


**FIGURE 12.** Obtained PSD responses with respect to spectrum emission mask, maximum transmission power levels, MSE results, and achieved PAPR levels with respect to target PAPR levels are shown for 100 MHz 5G NR channel with 30 kHz SCS in (a), (b), (c), and (d), respectively. Both simulation-based and measured results are shown in (a)-(c).

FC-F-OFDM and, therefore, the 3 dB level is selected as the optimal level in this case. Results in Fig. 10(b) show that when the 5 MHz 5G NR channel is used, maximum transmission power levels are 26.7 dBm and 25.6 dBm for FC-F-OFDM and WOLA-OFDM, with target PAPR levels of 3 dB and 6 dB, respectively. When compared to the respective results shown in Table 3, which are 26.6 dBm and 25.4 dBm, we can claim that there is a strong correlation between measurement and simulation results, and in both cases FC-F-OFDM's performance advantage is clear.

For 20 MHz channel, the measurement results are shown in Fig. 11. The obtained PSD responses given in Fig. 11(a) show that a clearly higher transmission power can be achieved with FC-F-OFDM. Again, it is clear that the allocated band is efficiently used thanks to the FPE method. As seen from Fig. 11(c) and by following the logic of discussion given above for the 5 MHz channel, PAPR levels higher than 2.5 dB can be selected as targets for FC-F-OFDM whereas any level can be selected for WOLA-OFDM. When compared to the results of the 5 MHz channel case, clear reduction in mismatch between simulation and measurement results is also observed. Especially the PAPR target levels that result in high transmission power are accurately modeled by the simulator. Based on these observations and also results shown in Fig. 11(b), 26.5 dBm power level can be obtained with FC-F-OFDM by targeting a PAPR level of 3 dB. On the other hand, the achieved power level is 25.2 dBm with WOLA-OFDM by targeting at a PAPR level of 6 dB. Thus, the FC-F-OFDM provides a power advantage of 1.3 dBm. These results also validate the accuracy of the simulation results, where power levels are obtained as 26.5 dBm and 25.5 dBm, respectively.

As the final example, the 100 MHz channel case is considered and obtained results are given in Fig. 12. It can be seen from Fig. 12(a) that FC-F-OFDM provides clear transmission power advantage over WOLA-OFDM and emission performance is also better even though FC-F-OFDM is transmitted at a higher transmission power level. Similar to the results that pertain to the 5 MHz and 20 MHz channels, MSE is the main limiting factor for FC-F-OFDM and ACLR performance is the main problem for the WOLA-OFDM, where these limitations prevent higher transmission power levels. In this case, the optimal target PAPR levels for FC-F-OFDM and WOLA-OFDM waveforms are obtained as 3.4 dB

and 5.8 dB, respectively, and corresponding maximum transmission power levels are achieved as 25.8 dBm and 25 dBm, respectively. Difference between simulated and measured PA output power results is negligible except for the low target PAPR level results for FC-F-OFDM, where a gap of 0.5 dBm is observed. Beside this, it can be claimed that the obtained measurement results are close to the numerical ones and, as show in Table 3, resulting maximum transmission power leves are 26.3 dBm and 25.1 dBm, respectively.

Both numerical simulated and actual measured results demonstrate that FC-F-OFDM offers excellent emission performance and significant power efficiency improvement can be achieved by exploiting its emission performance advantages at a PA operation point near to saturation. For all the 5G NR transmission bandwidth configuration cases, approximately 1 dB higher transmission power level can be achieved with FC-F-OFDM waveform in comparison to WOLA-OFDM.

## VI. CONCLUSION

In this study, extensive transmission power analysis was provided for FC-F-OFDM and WOLA-OFDM waveforms. Since low PAPR is a key to achieve improvement in power efficiency, clipping was embedded into CP-OFDM signal generation. To improve the degradation in PAPR caused by FC filtering, a novel FPE based clipping noise allocation method was proposed for FC-F-OFDM. In the numerical evaluations, real PA effects were targeted and, therefore, a measured memory-polynomial model of the PA used in the testbed was generated. With this model, a simulator was created to analyze the maximum achievable transmission power levels for all possible maximum transmission bandwidth configurations defined in 5G NR. Moreover, various clipping levels were evaluated. To verify the obtained numerical results, an SDR-based testbed was also created and specific configuration cases were investigated in detail by using this testbed. As demonstrated with obtained numerical and experimental results, FC-F-OFDM provides significant transmission power advantage over WOLA-OFDM waveform.

## REFERENCES


[1] S. Parkvall, E. Dahlman, A. Furuskar, and M. Frenne, "NR: The new 5G radio access technology," *IEEE Commun. Standards Mag.*, vol. 1, no. 4, pp. 24–30, Dec. 2017.

[2] M. Shafi, A. F. Molisch, P. J. Smith, T. Haustein, P. Zhu, P. De Silva, F. Tufvesson, A. Benjebbour, and G. Wunder, "5G: A tutorial overview of standards, trials, challenges, deployment, and practice," *IEEE J. Sel. Areas Commun.*, vol. 35, no. 6, pp. 1201–1221, Jun. 2017.

[3] *NR; Overall description; Stage-2*, document 3GPP TS 38.300 Rel. 15 V15.4.0, Jan. 2019.

[4] E. Dahlman, S. Parkvall, and J. Sköld, *4G, LTE-Advanced Pro and The Road to 5G*. New York, NY, USA: Academic, 2016.

[5] A. Pitarokoilis, S. K. Mohammed, and E. G. Larsson, "On the optimality of single-carrier transmission in large-scale antenna systems," *IEEE Wireless Commun. Lett.*, vol. 1, no. 4, pp. 276–279, Aug. 2012.

[6] *IEEE Standard for Telecommunications and Information Exchange Between Systems—LAN/MAN Specific Requirements—Part 11: Wireless Medium Access Control (MAC) and Physical Layer (PHY) specifications: High Speed Physical Layer in the 5 GHz band*, Standard 802.11a-1999, Dec. 1999.

[7] E. Bala, J. Li, and R. Yang, "Shaping spectral leakage: A novel low-complexity transceiver architecture for cognitive radio," *IEEE Veh. Technol. Mag.*, vol. 8, no. 3, pp. 38–46, Sep. 2013.

[8] *Waveform Candidates*, document R1-162199, 3GPP TSG RAN WG1 meeting, Apr. 2016.

[9] *NR; User Equipment (UE) Radio Transmission and Reception; Part 1: Range 1 Standalone*, document Rel. 16 V16.0.0, Jun. 2019.

[10] Y. Cai, Z. Qin, F. Cui, G. Y. Li, and J. A. McCann, "Modulation and multiple access for 5G networks," *IEEE Commun. Surveys Tuts.*, vol. 20, no. 1, pp. 629–646, 1st Quart., 2018.

[11] P. Guan, D. Wu, T. Tian, J. Zhou, X. Zhang, L. Gu, A. Benjebbour, M. Iwabuchi, and Y. Kishiyama, "5G field trials: OFDM-based waveforms and mixed numerologies," *IEEE J. Sel. Areas Commun.*, vol. 35, no. 6, pp. 1234–1243, Jun. 2017.

[12] J. Yli-Kaakinen, T. Levanen, S. Valkonen, K. Pajukoski, J. Pirskanen, M. Renfors, and M. Valkama, "Efficient fast-convolution-based waveform processing for 5G physical layer," *IEEE J. Sel. Areas Commun.*, vol. 35, no. 6, pp. 1309–1326, Jun. 2017.

[13] X. Zhang, M. Jia, L. Chen, J. Ma, and J. Qiu, "Filtered-OFDM–enabler for flexible waveform in the 5th generation cellular networks," in *Proc. IEEE Global Commun. Conf. (GLOBECOM)*, Dec. 2015, pp. 1–6.

[14] A. Zaidi, X. Chen, F. Athley, U. Gustavsson, J. Medbo, and G. Durisi, *5G Physical Layer: Principles, Models and Technology Components*. Amsterdam, The Netherlands: Elsevier, 2018.

[15] R. Ahmed, F. Schaich, and T. Wild, "OFDM enhancements for 5G based on filtering and windowing," in *Multiple Access Techniques for 5G Wireless Networks and Beyond*, M. Vaezi, Z. Ding, and H. Poor, Eds. Cham, Switzerland: Springer, 2018.

[16] R. Gerzaguet, N. Bartzoudis, L. G. Baltar, V. Berg, J.-B. Doré, D. Kténas, O. Font-Bach, X. Mestre, M. Payaró, M. Färber, and K. Roth, "The 5G candidate waveform race: A comparison of complexity and performance," *EURASIP J. Wireless Commun. Netw.*, vol. 2017, no. 1, p. 13, Dec. 2017, doi: 10.1186/s13638-016-0792-0.

[17] D. Garcia-Roger, J. F. de Valgas, J. F. Monserrat, N. Cardona, and N. Incardona, "Hardware testbed for sidelink transmission of 5G waveforms without synchronization," in *Proc. IEEE 27th Annu. Int. Symp. Pers., Indoor, Mobile Radio Commun. (PIMRC)*, Sep. 2016, pp. 1–6.

[18] O. Font-Bach, N. Bartzoudis, X. Mestre, D. Lopez-Bueno, P. Mege, L. Martinod, V. Ringset, and T. A. Myrvoll, "When SDR meets a 5G candidate waveform: Agile use of fragmented spectrum and interference protection in PMR networks," *IEEE Wireless Commun.*, vol. 22, no. 6, pp. 56–66, Dec. 2015.

[19] R. Zayani, H. Shaiek, X. Cheng, X. Fu, C. Alexandre, and D. Roviras, "Experimental testbed of post-OFDM waveforms toward future wireless networks," *IEEE Access*, vol. 6, pp. 67665–67680, 2018.

[20] M. Renfors, J. Yli-Kaakinen, T. Levanen, M. Valkama, T. Ihalainen, and J. Vihriala, "Efficient fast-convolution implementation of filtered CP-OFDM waveform processing for 5G," in *Proc. IEEE Globecom Workshops (GC Wkshps)*, Dec. 2015, pp. 1–7.

[21] T. Levanen, J. Pirskanen, K. Pajukoski, M. Renfors, and M. Valkama, "Transparent TX and TX waveform processing for 5G new radio mobile communications," *IEEE Wireless Commun.*, vol. 26, no. 1, pp. 128–136, Feb. 2019.

[22] G. Berardinelli, F. M. L. Tavares, T. B. Sorensen, P. Mogensen, and K. Pajukoski, "Zero-tail DFT-spread-OFDM signals," in *Proc. IEEE Globecom Workshops (GC Wkshps)*, Dec. 2013, pp. 229–234.

[23] R. Xu, L. Wang, Z. Geng, H. Deng, L. Peng, and L. Zhang, "A unitary precoder for optimizing spectrum and PAPR characteristic of OFDMA signal," *IEEE Trans. Broadcast.*, vol. 64, no. 2, pp. 293–306, Jun. 2018.

[24] S. Gokceli, T. Levanen, J. Yli-Kaakinen, M. Turunen, M. Allen, T. Riihonen, A. Palin, M. Renfors, and M. Valkama, "Software-defined radio prototype for fast-convolution-based filtered OFDM in 5G NR," in *Proc. Eur. Conf. Netw. Commun. (EuCNC)*, Jun. 2019, pp. 235–240.

[25] S. Gokceli, T. Levanen, J. Yli-Kaakinen, T. Riihonen, M. Renfors, and M. Valkama, "PAPR reduction with mixed-numerology OFDM," *IEEE Wireless Commun. Lett.*, vol. 9, no. 1, pp. 21–25, Jan. 2020.

[26] H. Ochiai and H. Imai, "Performance analysis of deliberately clipped OFDM signals," *IEEE Trans. Commun.*, vol. 50, no. 1, pp. 89–101, Jan. 2002.

[27] J. Armstrong, "Peak-to-average power reduction for OFDM by repeated clipping and frequency domain filtering," *Electron. Lett.*, vol. 38, no. 5, pp. 246–247, 2002.

[28] H. E. Rowe, "Memoryless nonlinearities with Gaussian inputs: Elementary results," *The Bell Syst. Tech. J.*, vol. 61, no. 7, pp. 1519–1525, Sep. 1982.

[29] J. Yli-Kaakinen, T. Levanen, A. Palin, M. Renfors, and M. Valkama, "Generalized fast-convolution-based filtered-OFDM: Techniques and application to 5G new radio," *IEEE Trans. Signal Process.*, vol. 68, pp. 1213–1228, 2020.
[30] H. Sorensen, M. Heideman, and C. Burrus, "On computing the split-radix FFT," *IEEE Trans. Acoust., Speech, Signal Process.*, vol. 34, no. 1, pp. 152–156, Feb. 1986.
[31] F. M. Ghannouchi and O. Hammi, "Behavioral modeling and predistortion," *IEEE Microw. Mag.*, vol. 10, no. 7, pp. 52–64, Dec. 2009.
[32] A. S. Tehrani, H. Cao, S. Afsardoost, T. Eriksson, M. Isaksson, and C. Fager, "A comparative analysis of the complexity/accuracy tradeoff in power amplifier behavioral models," *IEEE Trans. Microw. Theory Techn.*, vol. 58, no. 6, pp. 1510–1520, Jun. 2010.
[33] J. Kim and K. Konstantinou, "Digital predistortion of wideband signals based on power amplifier model with memory," *Electron. Lett.*, vol. 37, no. 23, p. 1417, 2001.
[34] *Specifications USRP-2954*, National Instruments, Austin, TX, USA, 2018. [Online]. Available: http://www.ni.com/pdf/manuals/375725c.pdf
[35] R. Schwarz. (2018). *NRP-Z11 Power Meter*. [Online]. Available: https://www.rohde-schwarz.com/fi/product/nrpz11-productstartpage_63493-8857.html
[36] (2018). *ZHL-4240+ Medium Power Amplifier*. [Online]. Available: http://www.minicircuits.com/pdfs/ZHL-4240+.pdf
[37] *Specifications VST PXIe-5840*, National Instrum., Austin, TX, USA, 2018. [Online]. Available: http://www.ni.com/pdf/manuals/376626c.pdf
[38] J. J. van de Beek, M. Sandell, and P. O. Borjesson, "ML estimation of time and frequency offset in OFDM systems," *IEEE Trans. Signal Process.*, vol. 45, no. 7, pp. 1800–1805, Jul. 1997.
[39] S. Coleri, M. Ergen, A. Puri, and A. Bahai, "Channel estimation techniques based on pilot arrangement in OFDM systems," *IEEE Trans. Broadcast.*, vol. 48, no. 3, pp. 223–229, Sep. 2002.

**SELAHATTIN GÖKCELI** (Student Member, IEEE) received the B.Sc. and M.Sc. degrees in electronics and communication engineering from Istanbul Technical University, Istanbul, Turkey, in 2015 and 2017, respectively. He is currently pursuing the D.Sc. degree with the Department of Electrical Engineering, Tampere University, Tampere, Finland.

His research interests include software-defined radio implementations, waveform design for 5G NR, PAPR reduction, and machine learning/artificial intelligence applications for physical layer of 5G NR.

**PABLO PASCUAL CAMPO** (Student Member, IEEE) received the B.Sc. degree in telecommunications and the M.Sc. degree in electrical engineering from Universidad Politécnica de Madrid, Madrid, Spain, in 2016 and 2018, respectively. He is currently pursuing the D.Sc. degree with the Department of Electrical Engineering, Tampere University, Tampere, Finland.

His research interests include digital predistortion, full-duplex systems and applications, and signal processing for wireless communications in the mmWave spectrum.

**TONI LEVANEN** (Member, IEEE) received the M.Sc. and D.Sc. degrees from the Tampere University of Technology (TUT), Finland, in 2007 and 2014, respectively. He is currently with the Department of Electrical Engineering, Tampere University.

In addition to his contributions in academic research, he has worked in industry on wide variety of development and research projects. His current research interests include physical layer design for 5G NR, interference modeling in 5G cells, and high-mobility support in millimeter-wave communications.

**JUHA YLI-KAAKINEN** received the Diploma Engineering degree in electrical engineering and the Doctor of Technology (Hons.) degree from the Tampere University of Technology (TUT), Tampere, Finland, in 1998 and 2002, respectively.

Since 1995, he has held various research positions with TUT. His research interests are in digital signal processing, especially in digital filter and filter-bank optimization for communication systems and very large-scale integration implementations.

**MATIAS TURUNEN** (Member, IEEE) is currently pursuing the M.Sc. degree in electrical engineering with Tampere University (TAU), Tampere, Finland.

He is currently a Research Assistant with the Department of Electrical Engineering, TAU. His current research interests include in-band full-duplex radios with an emphasis on analog RF cancellation, OFDM radar, and 5G new radio systems.

**MARKUS ALLÉN** was born in Ypäjä, Finland, in 1985. He received the B.Sc., M.Sc., and D.Sc. degrees in signal processing and communications engineering from the Tampere University of Technology (TUT), Tampere, Finland, in 2008, 2010, and 2015, respectively.

He is currently with the Faculty of Information Technology and Communication Sciences, Tampere University, as a University Instructor. His current research interests include software-defined radios, 5G-related RF measurements, and digital signal processing for radio transceiver linearization.

**TANELI RIIHONEN** (Member, IEEE) received the D.Sc. degree (Hons.) in electrical engineering from Aalto University, Helsinki, Finland, in August 2014.

From September 2005 to December 2017, he held various research positions at the School of Electrical Engineering, Aalto University. From November 2014 to December 2015, he was a Visiting Associate Research Scientist and an Adjunct Assistant Professor with Columbia University, New York, NY, USA. He is currently an Assistant Professor (tenure track) with the Faculty of Information Technology and Communication Sciences, Tampere University, Tampere, Finland. His current research interests include physical-layer OFDM (A), multiantennas, and relaying and full-duplex wireless techniques, especially the evolution of beyond 5G systems.

Dr. Riihonen was a recipient of the Finnish Technical Sector's Award for the Best Doctoral Dissertation of the year in Finland within all engineering sciences and the EURASIP Best Ph.D. Thesis Award 2017. He has been nominated 11 times as an Exemplary/Top Reviewer of various IEEE journals. He served as an Editor for the IEEE COMMUNICATIONS LETTERS, from October 2014 to January 2019. He has been serving as an Editor for the IEEE COMMUNICATIONS LETTERS, since May 2017.

**ARTO PALIN** (Member, IEEE) received the M.Sc. (Tech.) degree from the Tampere University of Technology. He has long industrial experience in wireless technologies, covering cellular networks, broadcast systems, and local area communications. He is currently working as a Technical Leader with Nokia Mobile Networks, Finland, in the area of 5G SoC architectures.

**MARKKU RENFORS** (Life Fellow, IEEE) received the D.Tech. degree from the Tampere University of Technology (TUT), Tampere, Finland, in 1982.

Since 1992, he has been a Professor with the Department of Electronics and Communications Engineering, TUT, where he was the Head, from 1992 to 2010. His research interests include filter-bank-based multicarrier systems and signal processing algorithms for flexible communications receivers and transmitters.

Dr. Renfors was a co-recipient of the Guillemin Cauer Award (together with T. Saramäki) from the IEEE Circuits and Systems Society, in 1987.

**MIKKO VALKAMA** (Senior Member, IEEE) received the M.Sc. and D.Sc. degrees (Hons.) in electrical engineering (EE) from the Tampere University of Technology (TUT), Tampere, Finland, in 2000 and 2001, respectively. His Ph.D. dissertation was focused on advanced I/Q signal processing for wideband receivers: models and algorithms.

In 2003, he was a Visiting Postdoctoral Research Fellow with the Communications Systems and Signal Processing Institute, San Diego State University (SDSU), San Diego, CA, USA. He is currently a Full Professor and the Department Head of Electrical Engineering with Tampere University (TAU), Tampere. His current research interests include radio communications, radio localization, and radio-based sensing, with particular emphasis on 5G and beyond mobile radio networks.

Dr. Valkama was a recipient of the Best Ph.D. Thesis Award of the Finnish Academy of Science and Letters for his Ph.D. dissertation.